Growth of Topological Insulator Bi₂Se₃ Particles on GaAs via Droplet Epitaxy

Sivakumar Vishnuvardhan Mambakkam¹, Saadia Nasir², Wilder Acuna¹, Joshua M. O. Zide¹,

and Stephanie Law^{1), 2), a)}

1) Department of Materials Science and Engineering, University of Delaware, 201 DuPont Hall, 127 The Green,

Newark, Delaware 19716

²⁾ Department of Physics and Astronomy, University of Delaware, 217 Sharp Lab, 104 The Green, Newark,

Delaware 19716

a) Electronic mail: slaw@udel.edu

Abstract

The discovery of topological insulators (TIs) and their unique electronic properties has motivated

research into a variety of applications, including quantum computing. It has been proposed that

TI surface states will be energetically discretized in a quantum dot nanoparticle. These

discretized states could then be used as basis states for a qubit that is more resistant to

decoherence. In this work, prototypical TI Bi₂Se₃ nanoparticles are grown on GaAs (001) using

the droplet epitaxy technique, and we demonstrate the control of nanoparticle height, area, and

density by changing the duration of bismuth deposition and substrate temperature. Within the

growth window studied, nanoparticles ranged from 5-15 nm tall with an 8-18nm equivalent

circular radius, and the density could be relatively well controlled by changing the substrate

temperature and bismuth deposition time.

Introduction

Topological insulators (TIs) are a class of materials which exhibit remarkable electronic

properties [1, 2, 3, 4]. This is due to the presence of heavy metals, resulting in strong spin-orbit

coupling. This spin-orbit coupling results in the bands overlapping, causing a rearrangement of

the bands, or band inversion. This means the symmetry within both the conduction and valence

bands is flipped near the Gamma point in the Brillouin zone. When TIs contact materials with a

different symmetry, TI surface states form to satisfy the interfacial boundary conditions. These are electronic states which cross the bulk band gap of the TI and are physically located at the TI surfaces. Electrons occupying these states have several unique properties: they are delocalized on the surface of the TI, they are nearly massless, and they are spin-momentum locked. Altogether, this makes electrons occupying these states resistant to scattering into other surface states in the absence of a magnetic perturbation. This behavior has motivated interest in TIs in a variety of contexts such as spintronic or optoelectronic devices [5, 6].

One application for TIs is creating quantum dots to serve as room temperature quantum bits or "qubits". When reduced to nanoscale dimensions, the TI surface states are predicted to become quantized [7, 8]. These quantized states could serve as the qubit basis states. The reduced scattering pathways could then reduce qubit decoherence, potentially leading to room-temperature operation. Before creating devices, however, we must first answer two questions: 1) How do we produce the uniform TI nanoparticles needed to reduce inhomogeneous broadening and 2) Do the TI nanoparticles show evidence of quantized surface states? The work discussed in this paper focuses on answering the first question.

There are a variety of methods by which TI nanoparticles can be made. In this work, we use a growth technique called "droplet epitaxy" to produce Bi₂Se₃ nanoparticles [9, 10, 11]. We start by exposing the substrate to a small amount of bismuth which does not wet the substrate while keeping the substrate at a relatively low temperature. This promotes the formation of 3D particles or "droplets". Next, the particles are exposed to an overpressure selenium. These atoms then incorporate into the nanoparticles, forming Bi₂Se₃ since this is the most stable compound in the Bi-Se phase diagram. Droplet epitaxy can therefore be used to form pure Bi₂Se₃ nanoparticles with no secondary phases. Related growth studies have been performed using both

metalorganic vapor phase epitaxy (MOVPE) and molecular beam epitaxy (MBE) to grow both bismuth droplets and bismuth selenide particles [12, 13, 14, 11].

In this paper, we discuss the growth of Bi₂Se₃ nanoparticles on GaAs via droplet epitaxy using molecular beam epitaxy (MBE). We varied the substrate temperature during bismuth deposition and the duration of bismuth exposure to understand how these parameters impact the final nanoparticle height, area, and density. The goal was to determine the extent to which TI nanoparticles could be repeatably and controllably grown. We show that the substrate temperature growth window was relatively small, approximately 35° C. Within this window, nanoparticle heights and areas were relatively similar within error bars, approximately 5-15 nm tall and 200-1000 nm² (equivalent circular radius of approximately 8-18 nm) on average. The most consistently controllable variable was nanoparticle density, which increased with increasing bismuth exposure time and decreased somewhat with increasing substrate temperature. Overall, we demonstrate control over nanoparticle dimensions but within a somewhat narrow range.

Experimental Procedure

Samples were synthesized using a Veeco GenXplor MBE system in the University of Delaware Materials Growth Facility. Samples were grown on epi-ready (001) GaAs wafers. Wafers were loaded into the chamber and heated to 760-770 °C to desorb the oxide layer. To prevent gallium droplet formation during oxide desorption, a selenium overpressure of 7.5-9.6 x 10⁻⁶ Torr was used, as measured by beam flux monitoring (BFM). The selenium flux was started once the substrate temperature exceeded 300 °C. After bringing the substrate up to 770 °C, the substrate was cooled to the growth temperature. The selenium valve stayed open until the substrate dropped below 300 °C. All temperatures were measured by non-contact thermocouple.

A two-step process was used to grow the selenized bismuth nanoparticles. After the substrate stabilized at the desired initial growth temperature, the bismuth shutter was opened for between 20 to 100 seconds. The bismuth cell temperature was fixed at 480 °C, with a BFM-measured flux of 7.1-7.3 x 10⁻⁸ Torr. We exposed the substrate to a relatively small flux of bismuth, approximately 1.045 x 10¹³ atoms/(cm²s), to form 3-dimensional bismuth nanoparticles. Next, the bismuth shutter was closed, and the sample was annealed for between 100 to 20 seconds, such that the total time of bismuth deposition plus annealing is fixed at 120 seconds. Finally, the substrate temperature was lowered to 50 °C (ramp rate of 20 °C/min.) and the selenium shutter was opened, with a BFM flux of 3.5-5.3 x 10⁻⁶ Torr, forming Bi₂Se₃ nanoparticles. Selenium is kept open as the substrate cools and is closed once the substrate cools below 200 °C. The duration of selenium exposure varies, with growths done at 250 °C taking 6-7 minutes to cool, and growths done at 275/285 °C taking 9-10 minutes to cool. After selenium is closed, the sample is removed from the chamber for analysis.

Two parameters were varied to tune the nanoparticle area, height, and density: the duration of bismuth deposition (t_{Bi}) and the temperature of the substrate used for initial bismuth deposition (T_{sub}) . After growth, samples were examined using atomic force microscopy (AFM) and scanning electron microscopy (SEM). AFM was conducted using the Dimension-3100 V SPM system in the Keck Center for Advanced Microscopy and Microanalysis, and SEM was done using the Zeiss Merlin SEM system in the UD Nanofabrication Facility cleanroom. Quantities of interest for our study are nanoparticle height (by AFM), area (by SEM), and nanoparticle density per unit area (by AFM).

Results and Discussion

In this work, we studied growths done within the T_{sub} window of 250 to 285 °C, and with t_{Bi} between 20 and 100 seconds. As discussed in detail below, we discovered that substrates mounted on different plates experienced different actual temperatures even when the thermocouple read the same temperature. For this reason, we indicate the sample plate (Q2 or Q3) used for each sample. We will present data for a variety of pairs of samples grown with different bismuth deposition times or with different temperatures, then synthesize all results to form a picture of the dynamics of Bi₂Se₃ nanoparticle formation.

We first explored the properties of nanoparticles as a function of bismuth deposition time. Figure 1 shows data for the growths done at T_{sub}=285 °C: A (C) and B (D) are the AFM (SEM) images for growths done with t_{Bi}=20s and 100s, respectively. E and F summarize the statistical height and area data extracted from the AFM and SEM images, respectively. This information is presented in the form of box plots, which summarize multiple statistical quantities about the entire dataset. All box plots presented here include the following quantities: the box bounds the 25th to 75th percentile data, the line cutting through the box is the median, the solid square shows the mean, and the whiskers extend to the farthest datapoint that falls within the range of the Lower Inner and Upper Inner Fences (defined by 25th percentile minus 1.5*interquartile range, and 75th percentile plus 1.5*interquartile range, respectively). Solid diamonds above or below the plot represent outliers, some of which may be cut out of the plot for ease of viewing. See supplementary material at [URL will be inserted by AIP Publishing] for details on how AFM and SEM images were processed to obtain numerical data, as well as histograms of the datasets. AFM images were used to measure nanoparticle heights and density, and SEM images were used to measure nanoparticle area. Area data from AFM images was not used due to error caused by tip-sample convolution which may cause particles to seem larger in area than they are. The

densities of nanoparticles per unit area, as measured by AFM, is 1.53×10^{-5} particles/nm² for t_{Bi} =20s and 5.13×10^{-5} particles/nm² for t_{Bi} =100s (3.35 times more). For this pair of samples, within error bars, we see little to no change in average nanoparticle height. However, the sample with 100 seconds of bismuth deposition shows a notable increase in polydispersity, 1.6x increase in average area, and a 3x increase in nanoparticle density. By polydispersity, we refer to the relative number of nanoparticles which deviate from the average for a specific property, as well as the degree of their deviation. This can be expressed qualitatively by the change in the size of the box in the box plots or expressed quantitatively by statistical quantities like the standard deviation.

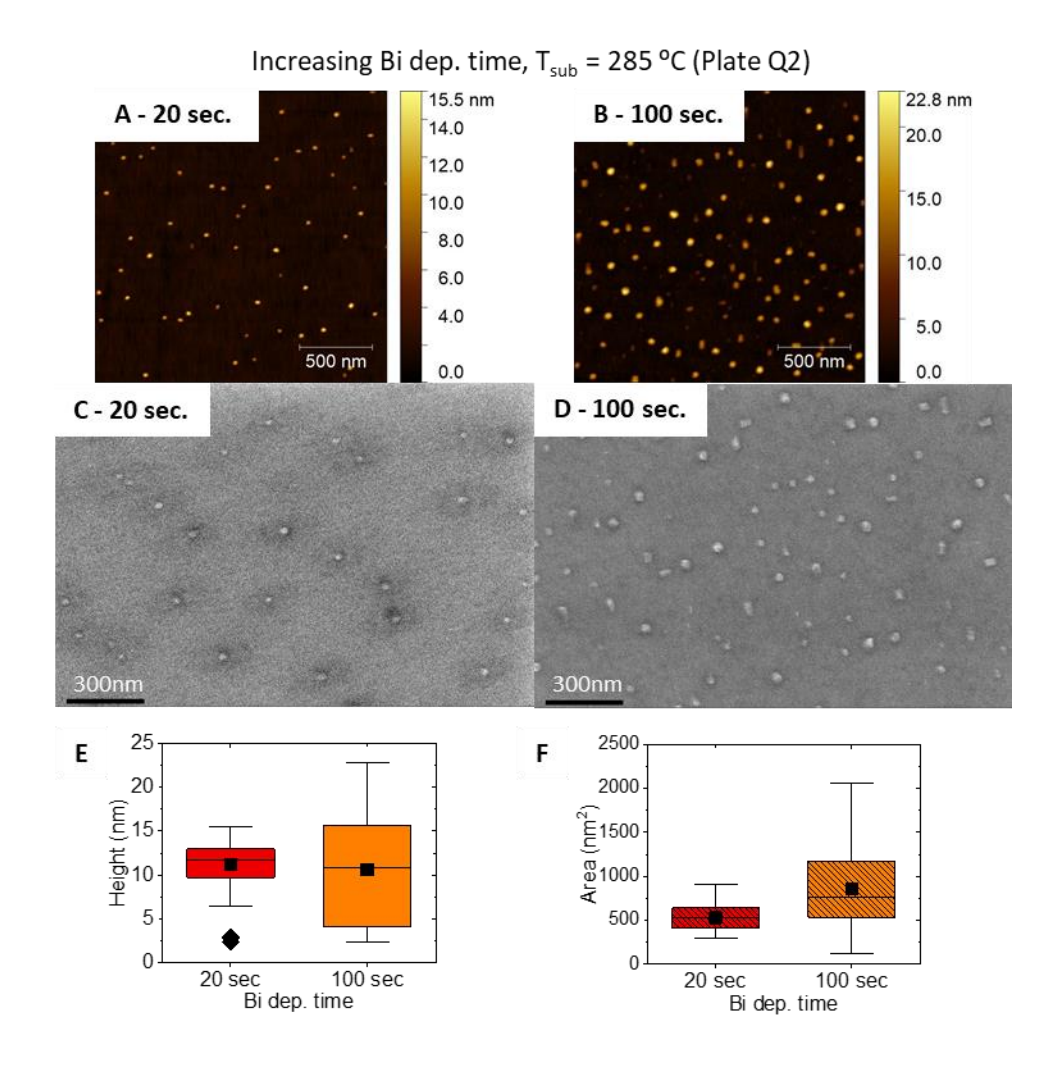


Figure 1: AFM and SEM images and resultant box plots for growths done at a T_{sub} of 285 °C with varying t_{Bi} . A and C are the AFM and SEM images for the growth done with 20 sec. t_{Bi} (grown 10/03/2020), B and D are the AFM and SEM images for the growth done with 100 sec. of t_{Bi} (grown 10/01/2020). E and F are the box plots showing height data from the AFM and area data from the SEM images respectively. Color scales and y-axes of box plots adjusted for ease of comparison (outliers in box plot may be cut out as a result).

Next, we compare four samples grown at T_{sub} =250 °C. Figure 2 shows the following: A (E), B (F), C (G) and D (H) are the AFM (SEM) images for samples with t_{Bi} =20s ,60s, 80s, and 100s, respectively. Fig. 2I and J summarize the statistical height and area data extracted from the AFM and SEM images, respectively. Density values for the growths are as follows: t_{Bi} =20s: 2.18 x 10⁻⁵ nm⁻²; t_{Bi} =60s: 12.8 x 10⁻⁵ nm⁻²; t_{Bi} =80s: 18.1 x 10⁻⁵ nm⁻²; and t_{Bi} =100s: 21.5 x 10⁻⁵ nm⁻². We note that the growth with t_{Bi} =20s had the selenium flux stopped at 255 °C as opposed to 300 °C.

to 36.3 nm due to an outlier). Third, the contrast in the SEM for Figure 2E was insufficient to perform an area analysis, and so this is omitted from the box plot. For this series, we continue to see a monotonic increase in density with bismuth deposition time, while nanoparticle height and area become progressively smaller.

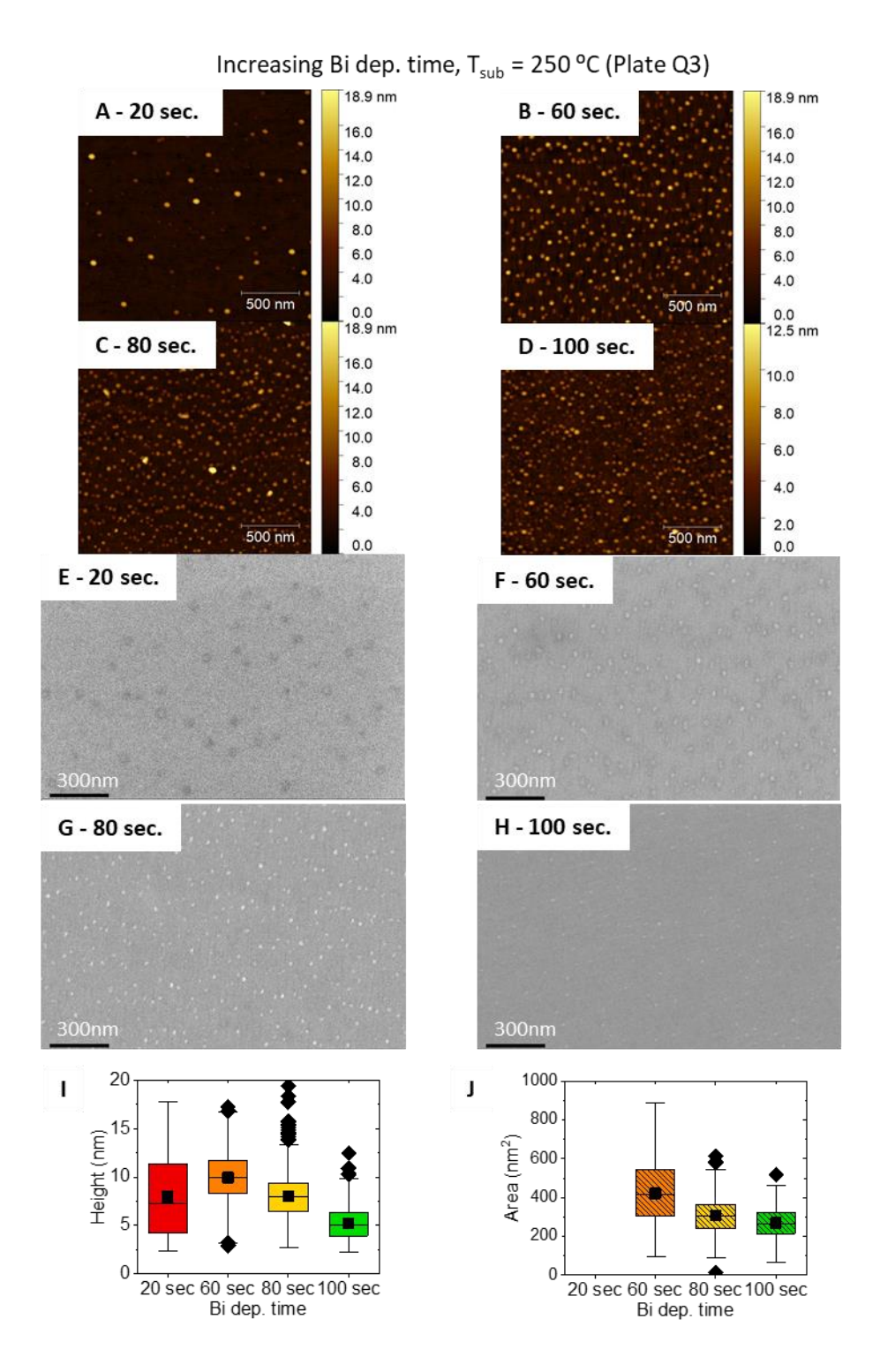


Figure 2: AFM and SEM images and resultant box plots for growths done at a T_{sub} of 250 °C with varying t_{Bi} . A)/E) are the AFM and SEM images for the growth done with 20 sec. t_{Bi} (grown 02/26/2021), B)/F) are the AFM and SEM images for the growth done with 60 sec. of t_{Bi} (grown 03/08/2021), C)/G) are the AFM and SEM images for the growth done with 80 sec. of t_{Bi} (grown 02/14/2021), D)/H) are the AFM and SEM images for the growth done with 100 sec. of t_{Bi} (grown 03/23/2021). I) and J) are the box plots showing height data from the AFM and area data

from the SEM images respectively. Color scales and y-axes of box plots adjusted for ease of comparison (outliers in box plot may be cut out as a result).

We now examine the effect of changing substrate temperature with a constant bismuth deposition time. We start with two growths done with t_{Bi} =100s, but with a substrate temperature difference of 10°C. Figure 3 shows data for the growths done with t_{Bi} =100s: A (C) and B (D) are the AFM (SEM) images corresponding to growths done at 275 and 285 °C, respectively. The nanoparticle density for the growth at t_{Bi} =100s and t_{Sub} =275 °C is 4.33 x 10⁻⁵ nm⁻², and for the growth done at t_{Sub} =285 °C is 5.13 x 10⁻⁵ nm⁻² (1.18 times more). The nanoparticle area, height, polydispersity, and density for both samples are the same to within error bars.

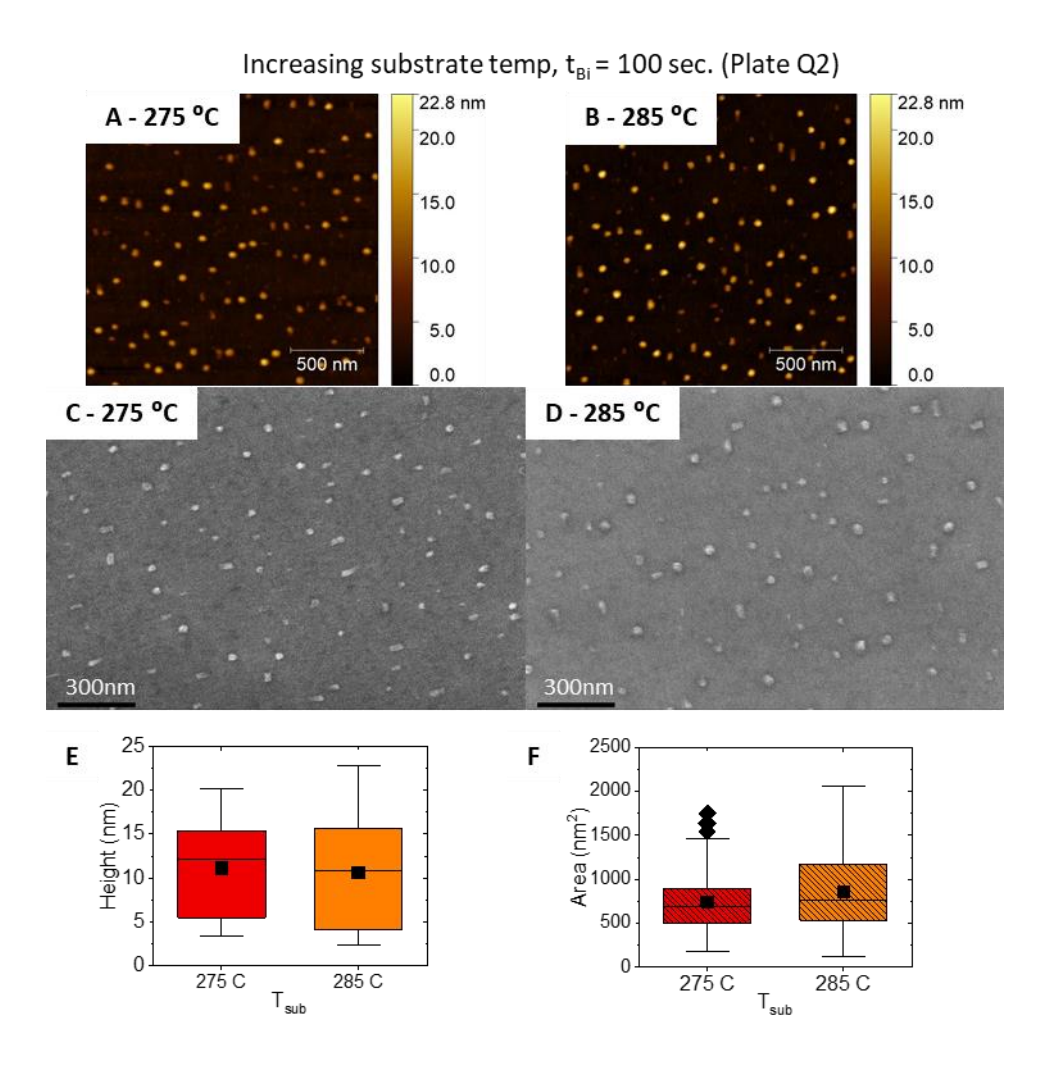


Figure 3: AFM and SEM images and resultant box plots for growths done with 100 sec. t_{Bi} and varying substrate temperature. A)/C) are the AFM and SEM images for the growth done at a T_{sub} of 275 °C (grown 09/25/2020),

B)/D) are the AFM and SEM images for the growth done at a T_{sub} of 285 °C (grown 10/01/2020). E) and F) are the box plots showing height data from the AFM and area data from the SEM images respectively. Color scales and y-axes of box plots adjusted for ease of comparison (outliers in box plot may be cut out as a result).

Now we look to another pair of growths, this time with t_{Bi}=60s, but with a larger temperature difference of 25 °C. Figure 4 shows the following: A (C) and B (D) are the AFM (SEM) images corresponding to growths done at 250 and 275 °C, respectively. The nanoparticle density for the growth at T_{sub}=250 °C is 8.98 x 10⁻⁵ nm⁻², and density for the growth done at T_{sub}=275 °C is 5.33 x 10⁻⁵ nm⁻² (0.59 times less). Unlike the previous case, we see a more significant change with the substrate temperature change. Average particle height increases by 1.43x and average particle area increases by 1.98x with increasing temperature.

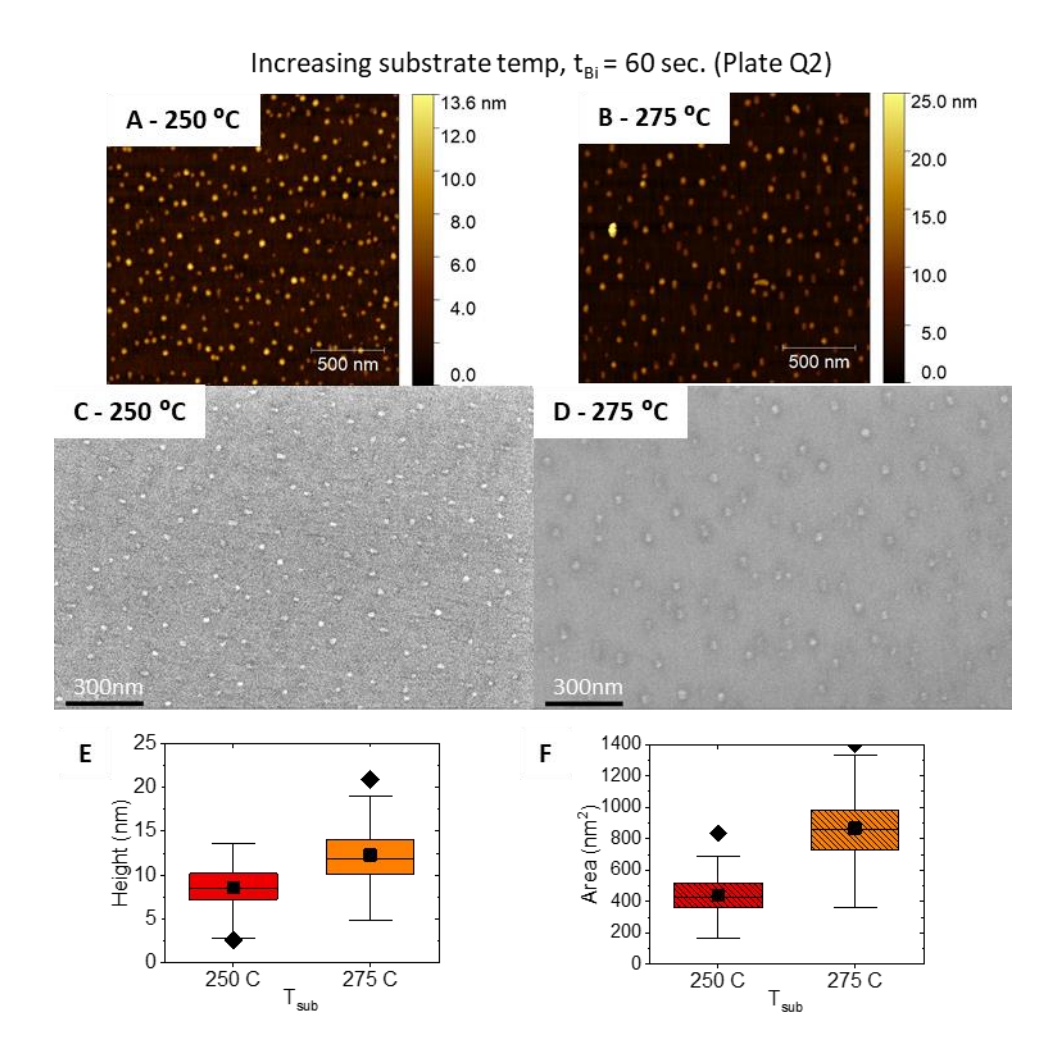


Figure 4: AFM and SEM images and resultant box plots for growths done with 60 sec. t_{Bi} and varying substrate temperature (plate Q2). A)/C) are the AFM and SEM images for the growth done at a T_{sub} of 250 °C (grown 02/26/2021), B)/D) are the AFM and SEM images for the growth done at a T_{sub} of 275 °C (grown 03/11/2021). E) and F) are the box plots showing height data from the AFM and area data from the SEM images respectively. Color scales and y-axes of box plots adjusted for ease of comparison (outliers in box plot may be cut out as a result).

Finally, we examine a series of three growths with t_{Bi}=60s, grown at 250°C, 275°C, and 285°C done on plate Q3. Figure 5 shows the following: A (D), B (E), and C (F) correspond to the AFM (SEM) images for the growths done at 250 °C, 275 °C, and 285 °C, respectively. Note that the scalebar in Figure 5B was adjusted for ease of comparison. Density for the growth at 250 °C is 12.8 x 10⁻⁵ nm⁻², 275 °C is 11.9 x 10⁻⁵ nm⁻², and 285 °C is 4.45 x 10⁻⁵ nm⁻². We again observe an increase in average nanoparticle area and height with increasing substrate temperature.

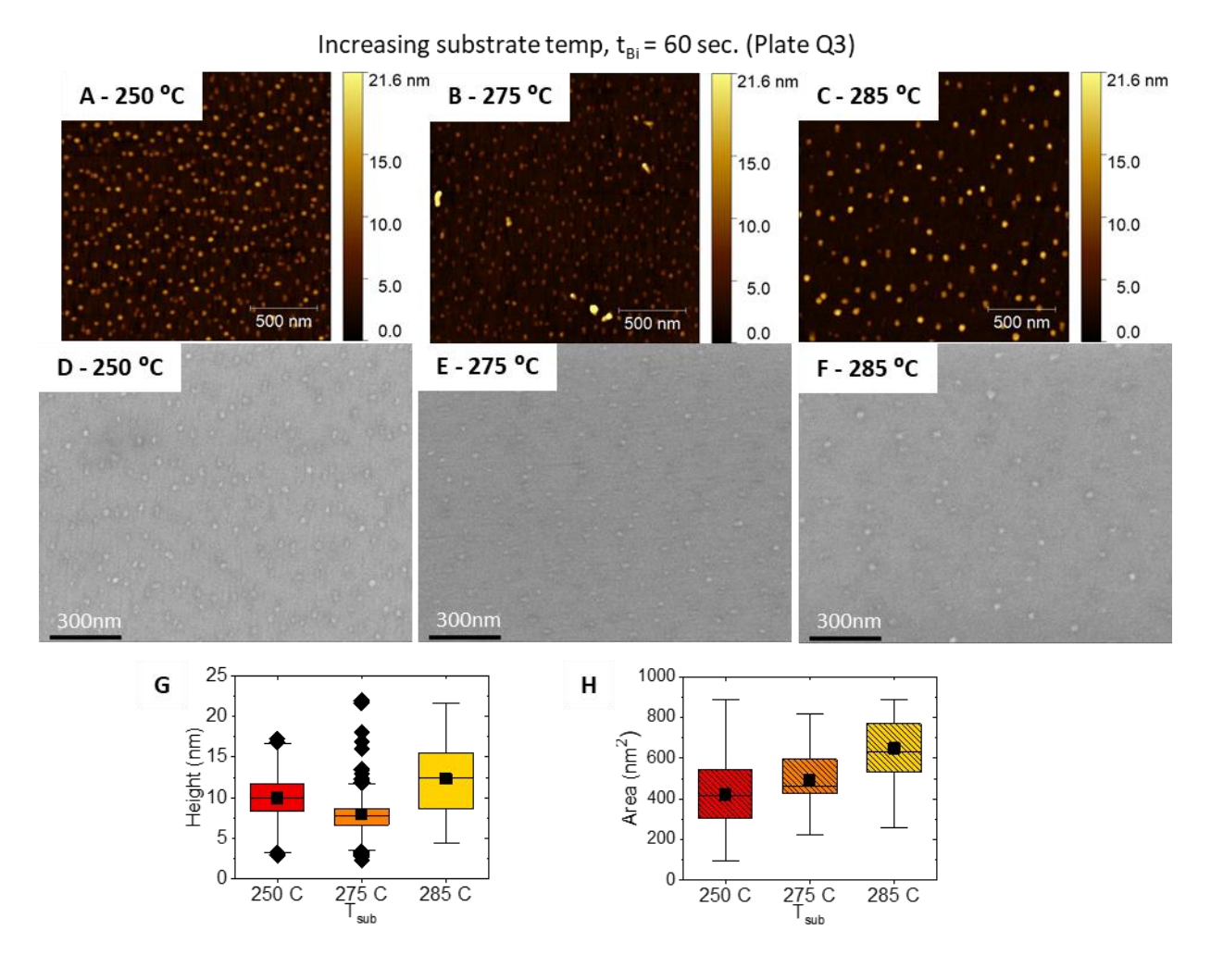


Figure 5: AFM and SEM images and resultant box plots for growths done with 60 sec. t_{Bi} and varying substrate temperature (plate Q3). A)/D) are the AFM and SEM images for the growth done at a T_{sub} of 250 °C (grown 03/08/2021), B)/E) are the AFM and SEM images for the growth done at a T_{sub} of 275 °C (grown 03/10/2021), and C)/F) are the AFM and SEM images for the growth done at a T_{sub} of 285 °C (grown 03/11/2021). G) and H) are the box plots showing height data from the AFM and area data from the SEM images respectively. SEM images were cropped. See supplementary material at [URL will be inserted by AIP Publishing] for full scans. Color scales and y-axes of box plots adjusted for ease of comparison (outliers in box plot may be cut out as a result).

Attempts were made to synthesize bismuth nanoparticles at both higher and lower substrate temperatures. The AFM scans for two attempts made at 225 °C and one at 325 °C are shown in Figure 6. All three samples showed a rough surface, and except for a single feature on Figure 6C and some short (<5 nm tall) features in Figure 6B, we did not show evidence of nanoparticle formation.

Growths at 225 °C and 325 °C

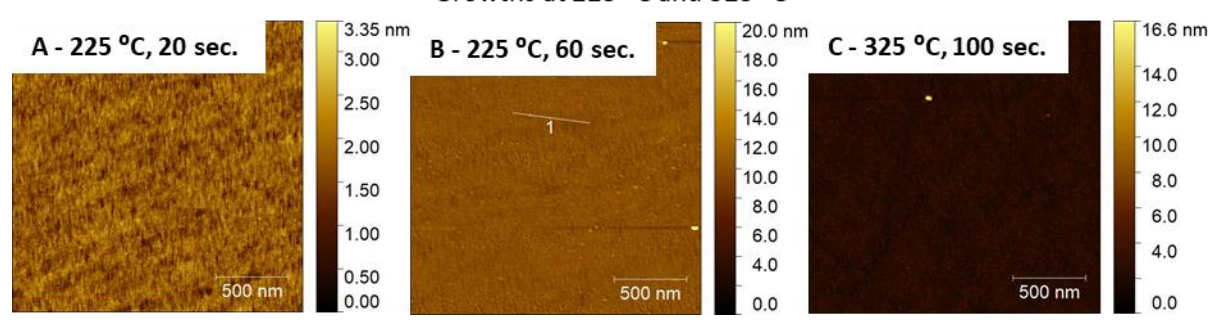


Figure 6: AFM images of growths performed at T_{sub} 's of 225 and 325 °C. A) is from a growth performed with 20 sec. t_{Bi} at a T_{sub} of 225 °C (plate Q3, 08/07/2020), B) is from a growth performed with 60 sec. t_{Bi} at a T_{sub} of 225 °C (plate Q2, 08/07/2020), and C) is from a growth performed with 100 sec. t_{Bi} at a T_{sub} of 325 °C (plate Q3, 12/17/2020). Color scales and y-axes of box plots adjusted for ease of comparison (outliers in box plot may be cut out as a result).

Discussion

We begin by discussing the series in Figures 1 and 2, which show trends of particle height and area with varying t_{Bi}. Neither of the series at 285 °C or 250 °C show changes in particle height and area within error bars as t_{Bi} changes. However, both show significant increases in particle density as t_{Bi} increases. This suggests that bismuth atoms upon impinging onto the surface are more likely to nucleate new particles as opposed to incorporate into existing ones. This trend is more dramatic for the growths done at lower substrate temperature, which supports this theory, as the mobility of the atoms on the substrate decreases with decreasing temperature, leading to more nucleation events.

Next, we consider the series in Figures 3, 4, and 5, which show trends of particle height and area with varying T_{sub}. In Figure 3, the series with a 10 °C difference, we see little change in particle properties, whereas in Figure 4, the series with a 25 °C difference, an increase in particle height and area is observed along with a decrease in particle density at higher temperatures. This is also seen in the full series from 250 to 285 °C shown in Figure 5. We note here the main difference between the growths in Figure 3 versus those in Figures 4 and 5 is the amount of bismuth

supplied: the growths in Figure 3 had t_{Bi} =100s, whereas the growths in Figures 4 and 5 all had t_{Bi} =60s. Overall, we observe that as the temperature increases, the nanoparticle height and area usually increase and the density decreases. This is not surprising. Since the amount of bismuth deposited is the same, if the particle area and height increase, the density must decrease. For higher temperatures, bismuth adatoms have a longer diffusion length, thus enabling the formation of larger particles rather than the nucleation of new particles. This density reduction with increasing substrate temperature was also observed by C. Li for bismuth droplets on GaAs grown via MBE [14]. However, this change in particle properties with increasing substrate temperature may also depend on the amount of bismuth deposited.

Now we consider the results for the growths done at 225 °C and 325 °C shown in Figure 6. In these growths, the only evidence of nanoparticle formation was a few short features in Figure 6B and one feature in Figure 6C. We therefore concluded that the substrate temperature window to achieve nanoparticle formation is small, less than 100°C. It is possible that the particles become increasingly more sparse on the substrate as the temperature increases and so it becomes increasingly difficult to detect them. This is potentially supported by recent AFM results made on the sample shown in Figure 6C, where taller, larger-area nanoparticle-like features (~100-120 nm tall, ~100 nm equivalent circular radii) are observed when increasing the scan size to 5x5 µm. Further work to identify the nature of these features is necessary, due to their large deviation from the features typically observed. Regardless, a more detailed study of the growth space between 285°C to 325 °C is needed.

Next, we will discuss the issue of reproducibility. Figure 7 shows two examples of repeated growths. The growths shown in Figure 7A and B were performed with t_{Bi} =100s at T_{sub} =250°C (on 09/25/2020 and 03/23/2021), and Figure 7D and E were performed with t_{Bi} =60s at

T_{sub}=285°C (on 10/03/2020 and 03/11/2021). Figure 7C and F are the respective height data box plots for each pair of growths showing the change with time. We observe a difference in nanoparticle height and area for the samples shown in Fig. 7A and B, indicating poor reproducibility, while we see similar nanoparticle height and area distributions for the samples shown in Fig. 7C and D, indicating good reproducibility.

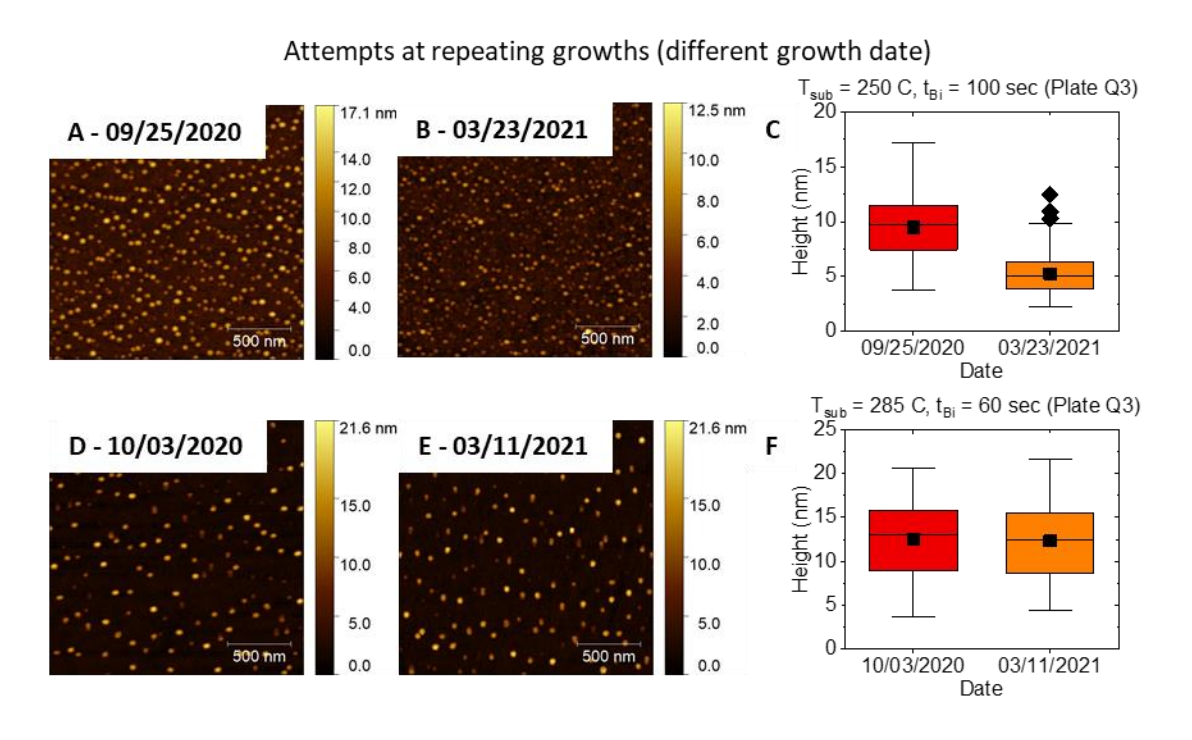


Figure 7: AFM images of repeated growths (grown on different days). A)/B) are for growths performed with 100 sec. t_{Bi} at a T_{sub} of 250 °C (plate Q3), D)/E) are for growths performed with 60 sec t_{Bi} at a T_{sub} of 285 °C (plate Q3). C)/F) are box plots showing height data for the pairs of A)/B) and D)/E) respectively. Color scales and y-axes of box plots adjusted for ease of comparison (outliers in box plot may be cut out as a result).

We attribute difficulties in reproducibility to the substrate holder becoming coated in selenium over time, causing a different physical substrate temperature for a similar thermocouple reading. This interpretation is supported by the difference in nanoparticle properties for growths performed with the same parameters, but on different substrate holders. We show two examples of this in Figure 8, with growths done on nearby growth days, but on different sample plates. The samples shown in Figure 8A and B were grown on 02/26/2021 and 03/08/2021 respectively, with

the sample shown in Figure 8A grown on plate Q2 and the sample shown in Figure 8B grown on plate Q3. Figure 8C is the height data box plot for the pair of growths in Figures 8A and B.

Nanoparticle densities for these growths are 8.98 x 10⁻⁵ nm⁻² and 12.8 x 10⁻⁵ nm⁻² for the samples shown in Figure 8A and B respectively. The samples shown in Figure 8D and E were grown on 03/11/2021 and 03/10/2021 respectively, with the sample shown in Figure 8D grown on plate Q2 and the sample shown in Figure 8E grown on plate Q3. Figure 8F is the height data box plot for the pair of growths in Figures 8D and E. Nanoparticle densities for these growths are 5.33 x 10⁻⁵ nm⁻² and 11.9 x 10⁻⁵ nm⁻² for the samples shown in Figures 8D and E respectively. From both the box plots and the density values, there is a clear difference in properties for growths done using different substrate holders. This has also been discussed in other growth studies published by our group [15].

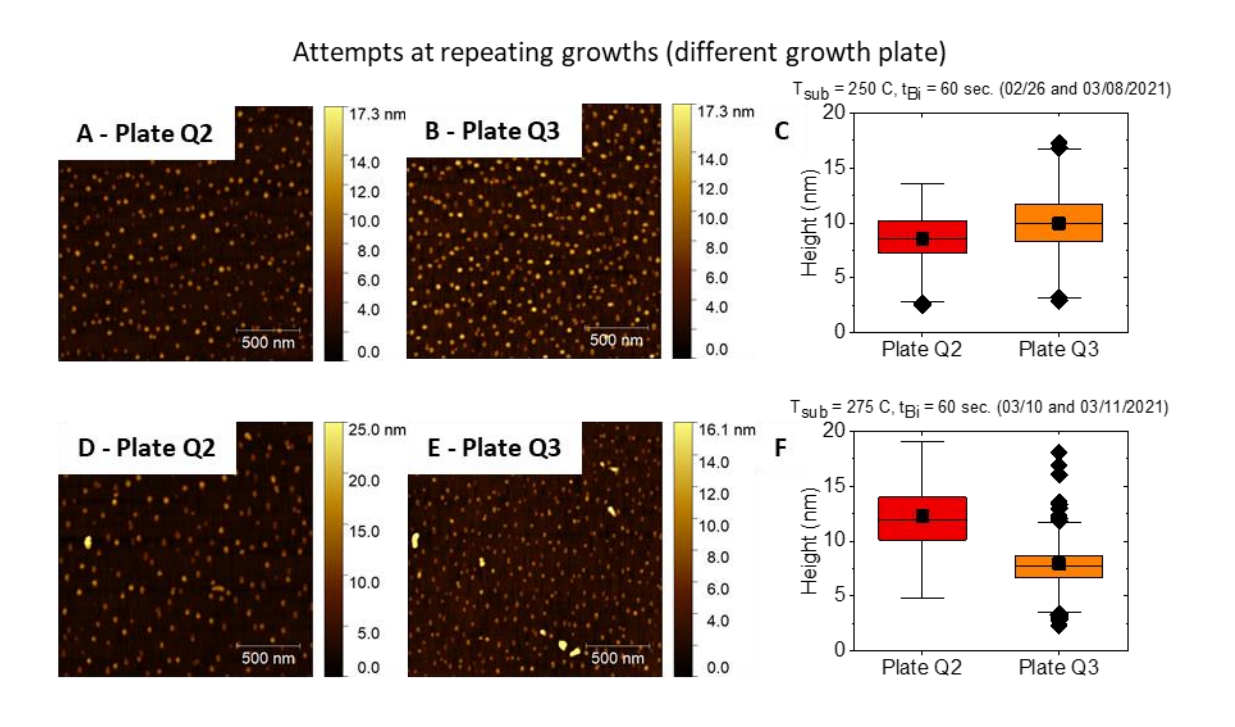


Figure 8: AFM images of repeated growths. A)/B) are for growths performed with 60 sec t_{Bi} at a T_{sub} of 250 °C (plate Q2 on 02/26/2021, plate Q3 on 03/08/2021), D)/E) are for growths performed with 60 sec. t_{Bi} at a T_{sub} of 275 °C (plate Q2 on 03/11/2021, plate Q3 on 03/10/2021). C)/F) are box plots showing height data for the pairs of A)/B) and D)/E) respectively. Color scales and y-axes of box plots adjusted for ease of comparison (outliers in box plot may be cut out as a result).

To estimate the deviation in physical temperature between sample plates Q2 and Q3, we used the temperature at which the oxide desorbed from our GaAs wafers which should always be the same physical temperature. We measured this temperature by heating the sample in increments of 5°C while using reflection high-energy electron diffraction (RHEED) to monitor the surface reconstruction. GaAs deoxidation occurs when the RHEED pattern transitions from rings to streaks. Using this method, we approximate the deviation between plate Q2 and Q3 to be between 0 and 10° C. This agrees with the data shown in Fig. 7. As shown in the previous section, growths done at 225 °C showed little to no evidence of nanoparticles. These growths were done on 08/07/2020. We have also presented data for samples grown at 250 °C which were gathered in the range 02/26/2021 to 03/23/2021, and these growths all showed clear presence of nanoparticles. We therefore believe that the shift in physical temperature due to successive growths is < 25 °C. We note that we have few datapoints for this deoxidation temperature and a relatively high uncertainty. In addition, the temperature deviation at the high temperatures of the deoxidation point (710-730 °C by thermocouple) may not be representative of the deviation at lower temperatures. However, we are confident that a change in physical temperature caused the difficulties in reproducibility. This highlights the extreme sensitivity of these samples to substrate temperature as well as the relatively narrow substrate temperature window.

Finally, we contrast the growth procedure and results presented in this work with previously published results. In particular, the growths of bismuth nanoparticles by C. Li et al. [14] and Bi₂Se₃ nanoparticles by M. Claro et al. [11] will be discussed. Both works use the technique of droplet epitaxy to form bismuth nanoparticles on GaAs, with the latter work extending the recipe to include selenium exposure to form Bi₂Se₃ nanoparticles. Both works provided a proof of

concept for creating nanoparticles of the kind we were interested in studying, and our approach was adapted from the ones discussed in these works.

The first point of contrast in our approach is the preparation of the initial GaAs substrate. As purchased, GaAs wafers have an epi-ready oxide layer on top which is desorbed at a high temperature prior to growth. This desorption is typically done under an overpressure of arsenic, to reduce the formation of gallium droplets and the surface roughness. Afterward, a GaAs overlayer is often grown to further improve the quality of the growth surface. This is the approach used in both aforementioned works.

However, for MBE growth chambers where selenium is used as a source, it is not recommended to have an arsenic source in the same chamber as there is the risk of arsenic substitution and incorporation in selenide materials due to their similar atomic radii. Therefore, for each growth described here the substrate would have to be transferred into an arsenide growth chamber for oxide desorption and GaAs growth, after which it would be transferred into the selenide growth chamber for the nanoparticle growth. This is the approach used in [11]. For the volume of growths required in our study, this approach was deemed to not be feasible in the short term. Therefore, as described in the Experimental Procedure section, we desorbed the epi-ready oxide under an overpressure of selenium, and this is the growth surface which was used for the growth of our nanoparticles.

This approach is not very well-studied. One study of the passivation of GaAs surfaces with selenium suggests that selenium can incorporate to form a stable surface [16], although their method for preparing the surface is not the same as what is done during desorption of the epiready oxide. Preliminary XPS measurements of our surfaces suggest that there is some selenium incorporation. We do also observe droplet-like features in SEM on a larger size scale than the

nanoparticle studied in this work. See supplementary material at [URL will be inserted by AIP Publishing] for more details on these as well as other features observed in the growths aside from the nanoparticles studied.

We expect that this difference in substrate preparation method plays a role in nanoparticle formation. We note that while the previously mentioned studies discuss growths with (1x3) and c(4x4) reconstructions of GaAs, we observe a (2x4) reconstruction using our method. We suspect that both the surface roughness and the number of dangling bonds on the surface are different for the surfaces prepared using a selenium overpressure. This would in turn affect the diffusion and nucleation of bismuth nanoparticles by changing the bonding at the substrate/nanoparticle interface. Specifically, with a possibly greater number of dangling bonds and several unsatisfied selenium bonds on the substrate surface, bismuth atoms may tend towards nucleating new particles by bonding with the selenium. This is at least partially supported by our observation of increased nanoparticle density with bismuth deposition time. This theory of stronger bonding at the nanoparticle/substrate interface could also explain why our attempts to remove these nanoparticles from GaAs substrates via sonication of the samples in solvents have failed, despite their nature as van der Waals materials. To verify this theory, a detailed TEM study of the nanoparticle/substrate interface is needed.

We also performed one growth in which the GaAs oxide layer was desorbed under an arsenic overpressure and a GaAs layer was grown, followed by transfer of the substrate under vacuum into our selenide growth chamber to perform the Bi₂Se₃ nanoparticle growths. We show in Figure 9 the AFM and SEM images for this growth, which was performed using a substrate temperature of 250°C and a bismuth deposition time of 60 seconds (all other parameters such as flux and approximate Bi:Se flux ratio are as described in the Experimental Procedure section).

We observe nanoparticles similar to those previously reported, with most between 10-20nm tall and with effective radii between 25-45nm. Compared to the nanoparticles grown on the selenium-prepared surfaces, these are generally taller, larger in area, and significantly less dense. The difference in morphology and density can likely be attributed to a smoother surface after the growth of the GaAs layer compared to the samples deoxidized under a selenium overpressure. A smoother surface will have fewer defects at which particles can nucleate as well as longer adatom diffusion lengths.

Growth of nanoparticles on smoother GaAs

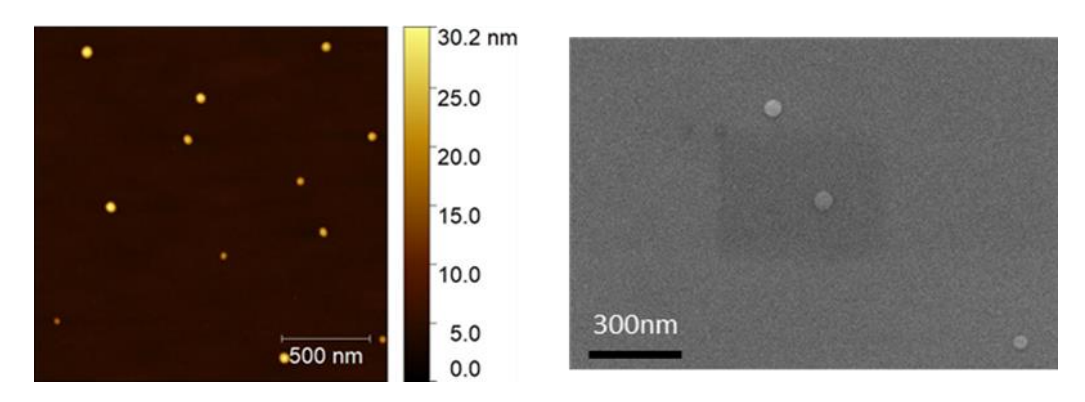


Figure 9: AFM and SEM images of growths performed on GaAs prepared by desorption under arsenic overpressure. Growths performed with 60 seconds of bismuth deposition at 250 °C.

Another deviation between our growths and previous reports are the exact details of the growth procedure. In principle, the growth of Bi/Bi₂Se₃ nanoparticles by droplet epitaxy is quite simple, and just involves the deposition of bismuth under conditions that promote nanoparticle formation, followed by (for the formation of Bi₂Se₃) sufficient selenium exposure to cause incorporation and crystallization. We summarize the growth procedures for the three works discussed so far in Table 1.

Table 1: Growth procedures for Bi/Bi2Se3 nanoparticles grown on GaAs(001) by MBE

Report	C. Li et al. (Bi	M. Claro et al. (Bi and	Our growth recipe
Growth	nanoparticles)	Bi ₂ Se ₃ nanoparticles)	
step			
Bismuth	Stabilization at	Stabilization at	Stabilization at substrate
deposition	substrate temperature	substrate temperature,	temperature for between
	for 30 minutes, then	then deposition with	11 and 27 minutes, then
	deposition with fixed	fixed bismuth flux until	deposition with a fixed
	bismuth flux for	GaAs RHEED pattern	bismuth flux. Total time
	between 10 to 35	was no longer visible	for this step is kept
	seconds (for fixed	(approximately 15	constant at 120 seconds,
	substrate temperature),	minutes).	with bismuth shutter
	and for 15 seconds (for		open for between 20 to
	varying substrate		100 seconds and
	temperature).		bismuth shutter closed
			for the remainder of the
			120 seconds.
Selenium	N/A	Closed bismuth shutter,	After 120 seconds
deposition		and immediately	"bismuth step",
		opened selenium	selenium shutter opened
		shutter at the same	and substrate
		substrate temperature	temperature setpoint set
		for 40 minutes.	to 50°C. Selenium

	shutter closed when
	substrate temperature
	reaches 200°C.

In this study, a different approach is used for both the bismuth and selenium deposition steps. For the bismuth deposition, a time of 120 seconds is fixed for the "bismuth" step wherein the bismuth shutter is opened for between 20 and 100 seconds and then is closed for the remainder of the 120 seconds. Therefore, there is a period of between 20 to 100 seconds following bismuth deposition where there is no flux exposed on the substrate while it sits at the initial substrate temperature. This was done based on the assumption that total growth time would play a role in determining the final characteristics of the nanoparticles, since while the substrate is being heated the motion of atoms on the surface is inevitable. Therefore, to study the variable of total bismuth deposition in isolation, we decided to perform the growth in this way to decouple it from the variable of total growth time as much as possible.

For the selenium deposition step, the selenium shutter was opened while at the same time the substrate temperature setpoint was set to 50°C. The purpose of this was to set the setpoint low enough such that the PID controlling the power outputted to the substrate heater would decrease the output to 0%, stopping heating to the substrate. We assume thus that the motion of the previously deposited bismuth becomes sufficiently slowed and the main process occurring during this time is the diffusion and incorporation of selenium into the bismuth nanoparticles. The selenium shutter is closed when the substrate temperature reaches 200°C. This takes between 6-9 minutes depending on the initial substrate temperature. It is common practice in our group based on experience growing Bi₂Se₃ thin films to maintain a selenium overpressure while

the substrate is above 200°C to prevent selenium desorption due to its high vapor pressure, and thus this was done for our nanoparticle growths as well.

The final aspects to compare are the growth results. Our nanoparticles are roughly the same height as both the bismuth and bismuth selenide nanoparticles mentioned in both reports (roughly 5-15nm), although the bismuth nanoparticles discussed in the work of M. Claro et al. prior to performing selenization were somewhat taller (~29nm). In terms of area/equivalent diameter, our nanoparticles are in a similar range if not somewhat smaller than those previously reported (<36nm, as opposed to ~50nm in diameter reported in previous work). However, our estimates of nanoparticle diameter are based on SEM measurements, previous reports relied on AFM results. As AFM tips themselves are roughly 10nm in diameter, the sample-tip convolution could lead to the deviation between our results and previously-reported results. As for observed trends, C. Li et al. studied the same trends of varying bismuth deposition time and substrate temperature. Like our study, they observed a decrease in nanoparticle density with increasing substrate temperature, accompanied by an increase in nanoparticle height. However, unlike our study, they did not observe a change in nanoparticle density with varying bismuth deposition time.

Conclusion

In this work, we showed that Bi₂Se₃ nanoparticles can be self-assembled on GaAs substrates using droplet epitaxy. We demonstrated control over the nanoparticle height, area, and density by controlling the bismuth deposition time and the substrate temperature. In general, the nanoparticles showed relatively small polydispersity, meaning that most particles were of the same area and height. We found that nanoparticles will only form in a relatively small substrate temperature window. These results show that while control over the nanoparticle size is possible,

there are limits on how large the particles can become using this method. For the nanoparticle size range presented (5-15 nm tall and 8-18 nm effective circular radius), theory indicates an energy level separation of ~0.05eV [8]. However, if the nanoparticle dimension is less than ~7nm, the wavefunction of the electrons occupying the surface states can tunnel through the nanoparticle and interfere with other quantized states [7]. The small size of the nanoparticles obtained by this method results in the largest energy separation of the quantized states, thus improving our chances of measuring them.

While larger particles may be possible, this would require changing one of the variables not accounted for in this study, for example moving outside of this substrate temperature window, changing the incoming bismuth flux, or changing the substrate or its preparation. We note that our group has attempted the production of similarly sized nanoparticles by means of e-beam lithography [17]. To achieve similar nanoparticle areas, heights, and densities requires a great deal of lithography time, and by extension expenditure. Therefore, this study shows the potential for creating TI nanoparticles over a large area via a relatively simple and inexpensive procedure, which will prove useful for future studies in harnessing TI surface states in devices.

Acknowledgements

S. V. M. and S. L. acknowledge funding from the National Science Foundation, Division of Materials Research under Award No. 1838504 and the Brookhaven National Laboratory/University of Delaware Seed Program under Award No. 20A00145. S. N. acknowledges funding from the U.S. Department of Energy, Office of Science, Office of Basic Energy Sciences, under Award No. DE-SC0017801. This research was partially supported by NSF through the University of Delaware Materials Research Science and Engineering Center DMR-2011824. The authors acknowledge the use of the Materials Growth Facility (MGF) at the

University of Delaware, which is partially supported by the National Science Foundation Major Research Instrumentation under Grant No. 1828141 and UD-CHARM, a National Science Foundation MRSEC under Award No. DMR-2011824.

Data Availability

Data supporting the work presented is available from corresponding authors upon reasonable request.

References

- [1] L. Fu, C. L. Kane and E. J. Mele, "Topological Insulators in Three Dimensions," *Phys. Rev. Lett.*, vol. 98, no. 10, pp. 1-4, 2007.
- [2] Y. Xia, D. Qian and e. al., "Observation of a large-gap topological-insulator class with a single Dirac cone on the surface," *Nat. Phys.*, vol. 5, pp. 398-402, 2009.
- [3] D. Hsieh, Y. Xia and e. al., "A tunable topological insulator in the spin helical Dirac transport regime," *Nature*, vol. 460, pp. 1101-1106, 2009.
- [4] Y. L. Chen, J. G. Analytis, J.-H. Chu and e. al., "Experimental Realization of a Three-Dimensional Topological Insulator, Bi2Te3," *Science*, vol. 325, pp. 178-181, 2009.
- [5] M. S. Rider, S. J. Palmer, S. R. Pocock, X. Xiao, P. A. Huidobro and V. Giannini, "A perspective on topological nanophotonics: Current status and future challenges," *J. Appl. Phys.*, vol. 125, no. 12, pp. 1-17, 2019.

- [6] T. Ginley, Y. Wang, Z. Wang and S. Law, "Dirac plasmons and beyond: the past, present, and future of plasmonics in 3D topological insulators," *MRS Comm.*, vol. 8, pp. 782-794, 2018.
- [7] G. Siroki, D. Lee, P. Haynes and e. al., "Single-electron induced surface plasmons on a topological nanoparticle," *Nat. Commun.*, vol. 7, 2016.
- [8] K. Imura, Y. Yoshimura, Y. Takane and T. Fukui, "Spherical topological insulator," *Phys. Rev. B*, vol. 86, 2012.
- [9] N. Koguchi and K. Ishige, "Growth of GaAs Epitaxial Microcrystals on an S-Terminated GaAs Substrate by Successive Irradiation of Ga and As Molecular Beams," *Jpn. J. Appl. Phys.*, vol. 32, pp. 2052-2058, 1993.
- [10] M. Gurioli, Z. Wang, A. Rastelli, T. Kuroda and S. Sanguinetti, "Droplet epitaxy of semiconductor nanostructures for quantum photonic devices," *Nat. Mat.*, vol. 18, pp. 799-810, 2019.
- [11] M. S. Claro, I. Levy, A. Gangopadhyay, D. J. Smith and M. C. Tamargo, "Self-assembled Bismuth Selenide (Bi2Se3) quantum dots grown by molecular beam epitaxy," *Sci. Rep.*, vol. 9, 2019.
- [12] H. Fitouri, I. Moussa, A. Rebey and B. E. Jani, "Surface analysis of different oriented GaAs substrates annealed under bismuth flow," *J. Cryst. Growth*, vol. 300, no. 2, pp. 347-352, 2007.
- [13] X. Lu, D. A. Beaton, R. B. Lewis, T. Tiedje and M. B. Whitwick, "Effect of molecular beam epitaxy growth conditions on the Bi content of GaAs1-xBix," *Appl. Phys. Lett.*, vol. 92, no. 19, 2008.
- [14] C. Li, Z. Q. Zeng, D. S. Fan and e. al., "Bismuth nano-droplets for group-V based molecular-beam droplet epitaxy," *Appl. Phys. Lett.*, vol. 99, no. 24, 2011.

- [15] P. T. Ginley, Y. Zhang, C. Ni and S. Law, "Epitaxial growth of Bi2Se3 in the (0015) orientation on GaAs (001)," *J. Vac. Sci. Technol. A*, vol. 38, pp. 1-7, 2020.
- [16] C. Gonzalez, I. Benito and e. al., "Selenium passivation of GaAs(001): a combined experimental and theoretical study," *J. Phys.: Condens. Matter*, vol. 16, pp. 2187-2206, 2004.
- [17] S. V. Mambakkam and S. Law, "Fabrication of topological insulator nanostructures," *J. Vac. Sci. Tech. B*, vol. 38, 2020.

Tables

Table 1: Growth procedures for Bi/Bi2Se3 nanoparticles grown on GaAs(001) by MBE

Report Growth step	C. Li et al. (Bi nanoparticles)	M. Claro et al. (Bi and Bi ₂ Se ₃ nanoparticles)	Our growth recipe
Bismuth deposition	Stabilization at substrate temperature for 30 minutes, then deposition with fixed bismuth flux for between 10 to 35 seconds (for fixed substrate temperature), and for 15 seconds (for varying substrate temperature).	Stabilization at substrate temperature, then deposition with fixed bismuth flux until GaAs RHEED pattern was no longer visible (approximately 15 minutes).	Stabilization at substrate temperature for between 11 and 27 minutes, then deposition with a fixed bismuth flux. Total time for this step is kept constant at 120 seconds, with bismuth shutter open for between 20 to 100 seconds and bismuth shutter closed for the remainder of the 120 seconds.
Selenium deposition	N/A	Closed bismuth shutter, and immediately opened selenium shutter at the same	After 120 seconds "bismuth step", selenium shutter opened and substrate

substrate temperature for 40 minutes.	temperature setpoint set to 50°C. Selenium shutter closed when substrate temperature reaches 200°C.
---------------------------------------	---

Figure captions

Figure 1: AFM and SEM images and resultant box plots for growths done at a T_{sub} of 285 °C with varying t_{Bi}. A and C are the AFM and SEM images for the growth done with 20 sec. t_{Bi} (grown 10/03/2020), B and D are the AFM and SEM images for the growth done with 100 sec. of t_{Bi} (grown 10/01/2020). E and F are the box plots showing height data from the AFM and area data from the SEM images respectively. Color scales and y-axes of box plots adjusted for ease of comparison (outliers in box plot may be cut out as a result).

Figure 2: AFM and SEM images and resultant box plots for growths done at a Tsub of 250 °C with varying tBi. A)/E) are the AFM and SEM images for the growth done with 20 sec. tBi (grown 02/26/2021), B)/F) are the AFM and SEM images for the growth done with 60 sec. of tBi (grown 03/08/2021), C)/G) are the AFM and SEM images for the growth done with 80 sec. of tBi (grown 02/14/2021), D)/H) are the AFM and SEM images for the growth done with 100 sec. of tBi (grown 03/23/2021). I) and J) are the box plots showing height data from the AFM and area data from the SEM images respectively. Color scales and y-axes of box plots adjusted for ease of comparison (outliers in box plot may be cut out as a result).

Figure 3: AFM and SEM images and resultant box plots for growths done with 100 sec. tBi and varying substrate temperature. A)/C) are the AFM and SEM images for the growth done at a Tsub of 275 °C (grown 09/25/2020), B)/D) are the AFM and SEM images for the growth done at a Tsub of 285 °C (grown 10/01/2020). E) and F) are the box plots showing height data from the AFM and area data from the SEM images respectively. Color scales and y-axes of box plots adjusted for ease of comparison (outliers in box plot may be cut out as a result).

Figure 4: AFM and SEM images and resultant box plots for growths done with 60 sec. tBi and varying substrate temperature (plate Q2). A)/C) are the AFM and SEM images for the growth done at a Tsub of 250 °C (grown 02/26/2021), B)/D) are the AFM and SEM images for the growth done at a Tsub of 275 °C (grown 03/11/2021). E) and F) are the box plots showing height data from the AFM and area data from the SEM images respectively. Color scales and y-axes of box plots adjusted for ease of comparison (outliers in box plot may be cut out as a result).

Figure 5: AFM and SEM images and resultant box plots for growths done with 60 sec. tBi and varying substrate temperature (plate Q3). A)/D) are the AFM and SEM images for the growth done at a Tsub of 250 °C (grown 03/08/2021), B)/E) are the AFM and SEM images for the growth done at a Tsub of 275 °C (grown 03/10/2021), and C)/F) are the AFM and SEM images for the growth done at a Tsub of 285 °C (grown 03/11/2021). G) and H) are the box plots showing height data from the AFM and area data from the SEM images respectively. SEM images were cropped. See supplementary material at [URL will be inserted by AIP Publishing]

for full scans. Color scales and y-axes of box plots adjusted for ease of comparison (outliers in box plot may be cut out as a result).

Figure 6: AFM images of growths performed at Tsub's of 225 and 325 °C. A) is from a growth performed with 20 sec. tBi at a Tsub of 225 °C (plate Q3, 08/07/2020), B) is from a growth performed with 60 sec. tBi at a Tsub of 225 °C (plate Q2, 08/07/2020), and C) is from a growth performed with 100 sec. tBi at a Tsub of 325 °C (plate Q3, 12/17/2020). Color scales and y-axes of box plots adjusted for ease of comparison (outliers in box plot may be cut out as a result).

Figure 7: AFM images of repeated growths (grown on different days). A)/B) are for growths performed with 100 sec. tBi at a Tsub of 250 °C (plate Q3), D)/E) are for growths performed with 60 sec tBi at a Tsub of 285 °C (plate Q3). C)/F) are box plots showing height data for the pairs of A)/B) and D)/E) respectively. Color scales and y-axes of box plots adjusted for ease of comparison (outliers in box plot may be cut out as a result).

Figure 8: AFM images of repeated growths. A)/B) are for growths performed with 60 sec tBi at a Tsub of 250 °C (plate Q2 on 02/26/2021, plate Q3 on 03/08/2021), D)/E) are for growths performed with 60 sec. tBi at a Tsub of 275 °C (plate Q2 on 03/11/2021, plate Q3 on 03/10/2021). C)/F) are box plots showing height data for the pairs of A)/B) and D)/E) respectively. Color scales and y-axes of box plots adjusted for ease of comparison (outliers in box plot may be cut out as a result).

Figure 9: AFM and SEM images of growths performed on GaAs prepared by desorption under arsenic overpressure. Growths performed with 60 seconds of bismuth deposition at 250 °C.

Growth of Topological Insulator Bi₂Se₃ Particles on GaAs via Droplet Epitaxy

Sivakumar Vishnuvardhan Mambakkam¹⁾, Saadia Nasir²⁾, Wilder Acuna¹⁾, Joshua M. O. Zide¹⁾, and Stephanie Law^{1), 2), a)}

- ¹⁾ Department of Materials Science and Engineering, University of Delaware, 201 DuPont Hall, 127 The Green, Newark, Delaware 19716
 - ²⁾ Department of Physics and Astronomy, University of Delaware, 217 Sharp Lab, 104 The Green, Newark, Delaware 19716
- a) Electronic mail: slaw@udel.edu

<u>Section 1 – Explanation of process used to analyze and extract numerical data from AFM and SEM images</u>

The following is an explanation of, and justification for, the process used to extract height data from the atomic force microscopy images of the selenized Bi droplets on GaAs. Data was processed using Gwyddion 2.56 (released 2020-06-30). The goal of the analysis is to correct common features of AFM data such as tilt, bowing and scan lines, while reducing the degree of data modification and prevent introduction of bias.

Example images shown throughout the process (from step 2 onwards) come from Sample #1099, for the AFM taken on 02-15-2021 (filename 1099 2um-majorflat-xaxis.004).

- 1. Import scan into Gwyddion.
- 1.5 In certain cases, the data upon importing the file will look as in Figure S1, where the scan looks very dark, with small lines or points which are very bright. This could occur due to errors in the scan where the reaction to the surface was discontinuous or interrupted. In order to proceed, we can use the "Correct horizontal scars (strokes)" function. This function should only be used in very rare cases, and only when the errors are clearly non-real, and not simply dissimilar from the features of interest (i.e. dust, unusually tall particles). In cases when it is used, it is noted how many times.

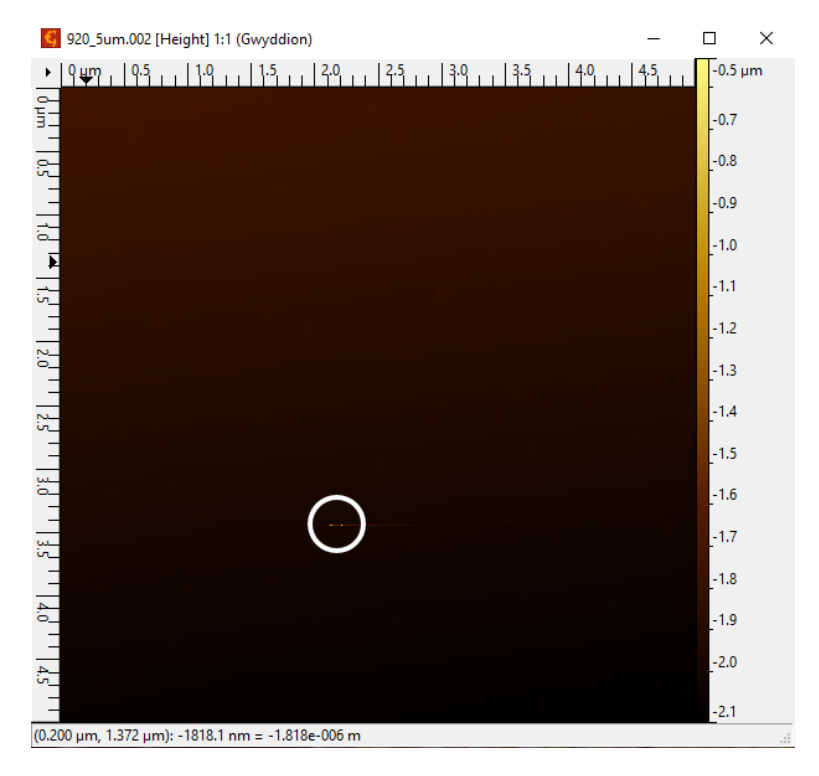


Figure S1: Initial image of 920_5um.002 upon uploading into Gwyddion, single scar biases the scalebar (inside of white circle)

2. The scan will appear to have a gradient over the recognizable data of the surface features of interest (i.e. the particles, Figure S2A). This can be recognized in both the scale bar, and in the 3-D view of the data in Figure S2B, as a large tilt in the data.

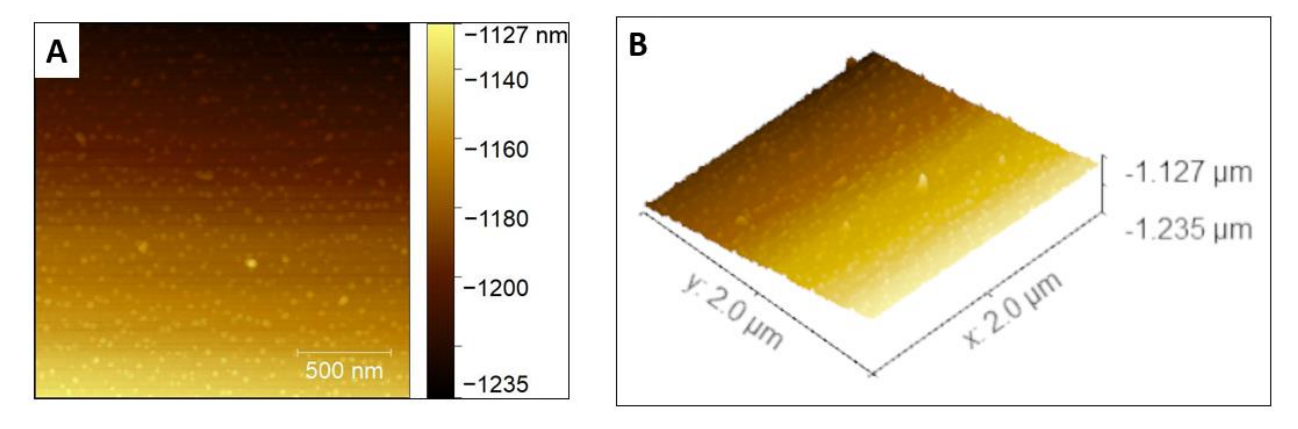


Figure S2: Initial image upon importing AFM data file into Gwyddion. A: planar view, B: 3-D view

To deal with this, we use the "Remove polynomial background" feature. This creates the model of the tilted plane with a user-defined polynomial in both x and y (Figure S3). For our study, we decided to fix the polynomial degree to 3 in both x and y directions. Lowering the polynomial fit degree more would make the fit less able to fully fit the tilt, while raising it too high risks modelling actual surface roughness that would then be subtracted, biasing the analysis. While a lower degree is generally better, raising the degree increased the fit and allowed for the data post-subtraction to be more suited to the subsequent steps which removed scanline effects.

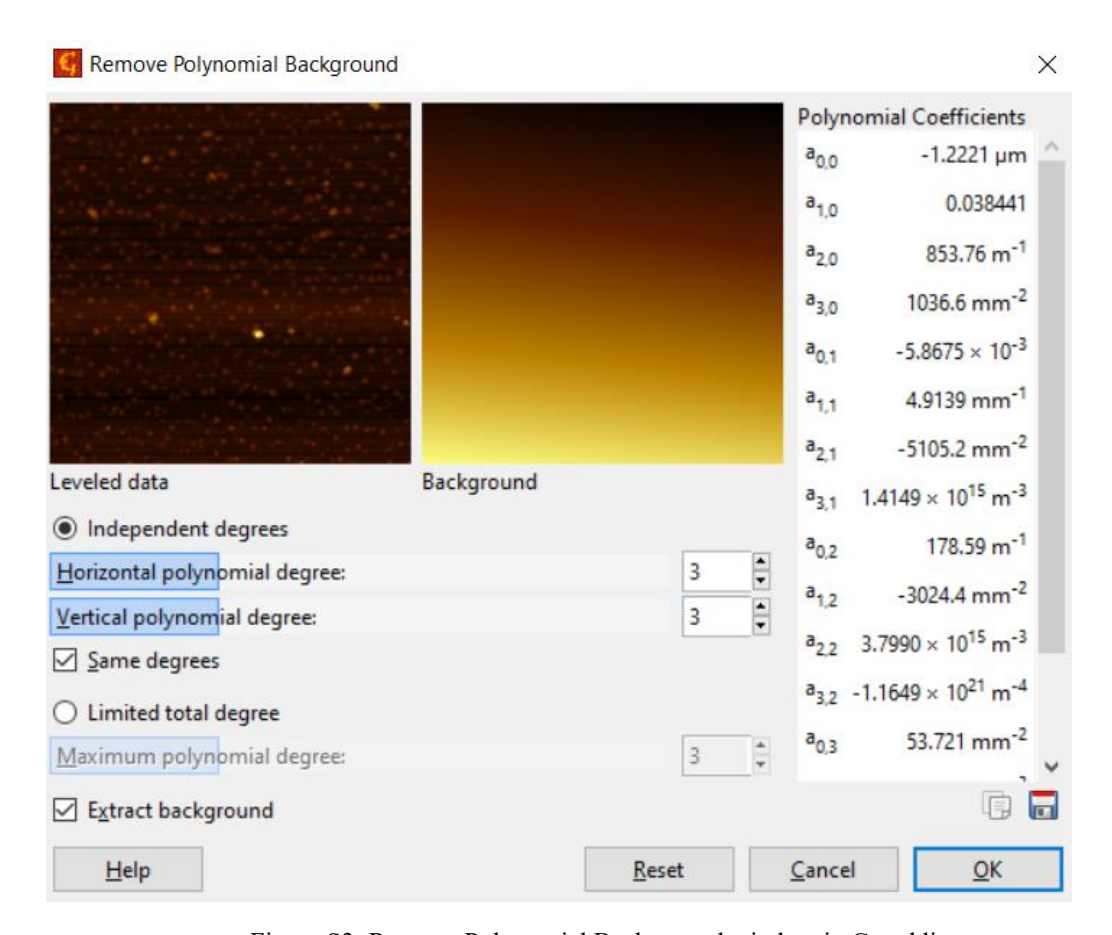


Figure S3: Remove Polynomial Background window in Gwyddion

3. There are lines crossing the scan in the x-direction, which come from scan lines which run in this direction and become obfuscated with the data. To correct this, we use the "Align rows using various methods" function. This tool takes the data along the scanlines, which is parallel to the scanning direction, and uses a characteristic function to fit onto the data and level it. Before we do this however, it is important to separate out the features of interest, as these can be affected by the leveling procedure. Our first step is to produce a mask over the features.

To create the mask, we use the "Mask by Segmentation" window (Figure S4). Here, we adjust several parameters until we have a mask over the features of interest. This is a process of trial and error to maximize to features covered. The scalebar may need to be adjusted prior to this by using the "Stretch color range to part of data" button to be able to see whether adjusting a parameter actually improves masking of shorter features.

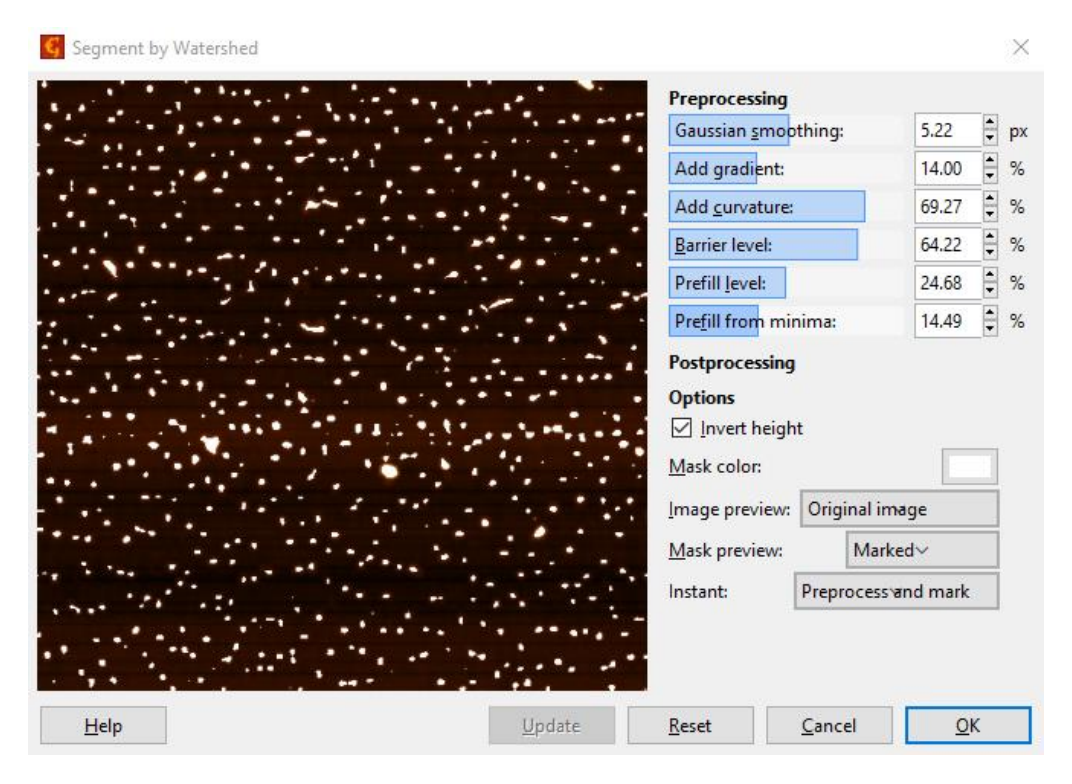


Figure S4: Mask by Segmentation window

Now the "Align rows" can be done (Figure S5). For our study, we used a Polynomial fit fixed at 1 degree to get a reasonable fit while minimizing data manipulation. Ensure that when the levelling is done, the "Exclude masked region" option is chosen at the bottom.

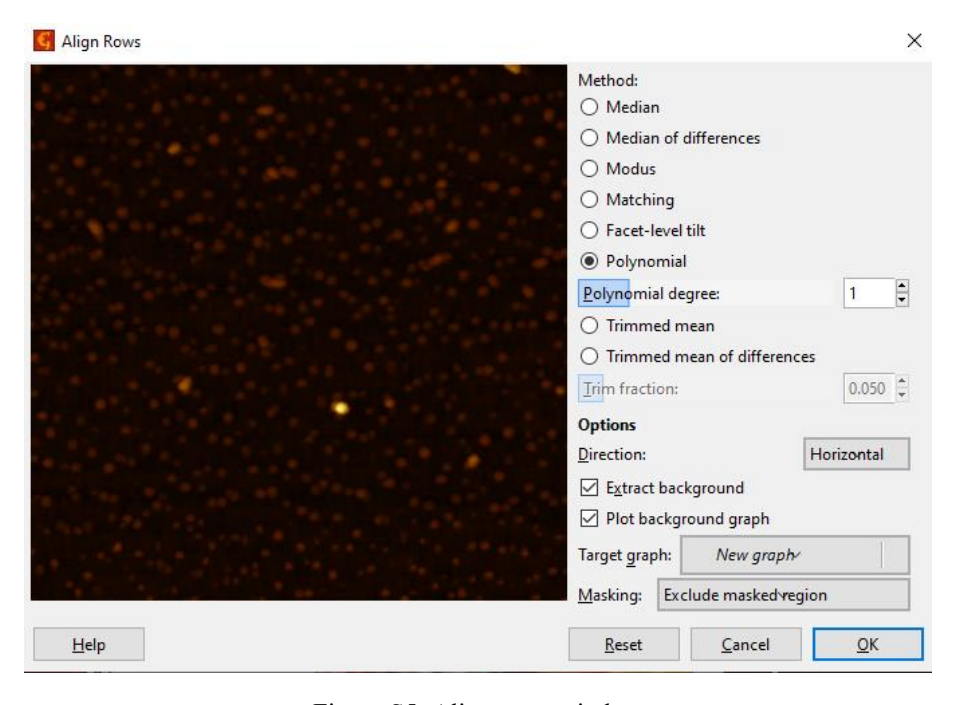


Figure S5: Align rows window

We can see the effect of this process below in Figure S6, showing the line-profile perpendicular to the scanning direction, and the 3-D view before and after aligning the rows. We can see that the shapes of the masked features of interest are not changed upon applying the Align Rows command. This is due to the use of the mask and the "exclude masked regions" option prior to performing the row alignment.

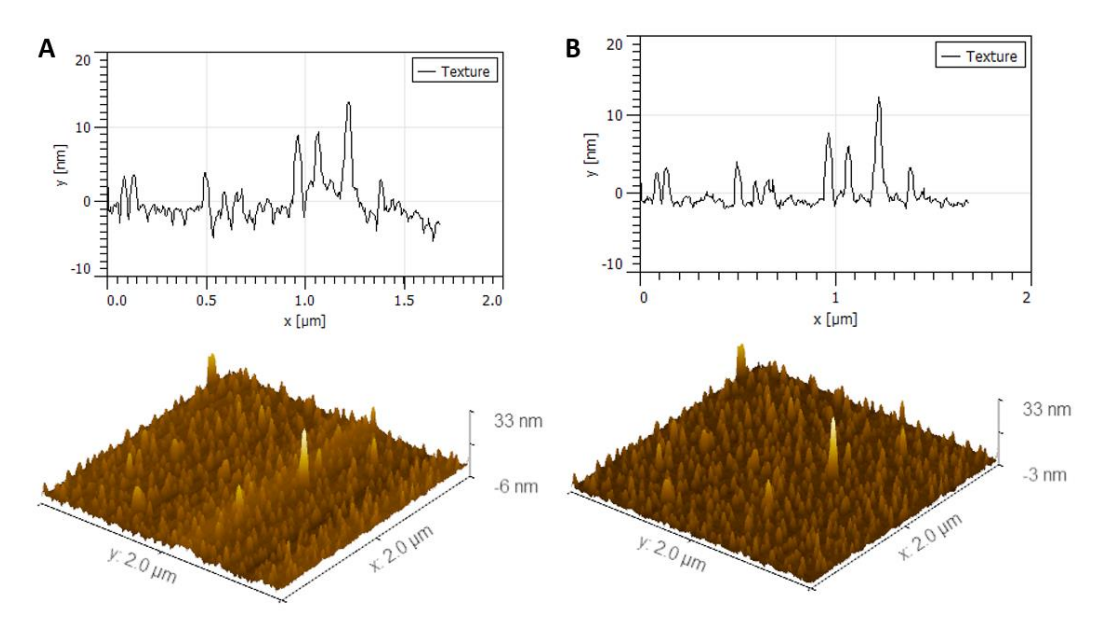


Figure S6: Line-profile and 3-D view of AFM image A) before and, B) after applying the Align Rows tool

5. Next the scale bar is shifted such that "0" is set at the bottom of the scalebar. This is done using the "Shift minimum data value to zero" button. Then, the height data for the features covered by the mask can be extracted using the "Distributions of various grain characteristics" button. In this window (Figure S7), multiple statistical quantities can be viewed and chosen using the check boxes. Whichever statistics are checked will be exported after the "Export raw data" radio box is filled and then "Okay" is clicked. The data will be exported as adjacent columns in .txt format, with each row corresponding to a specific masked feature, or "grain" by the nomenclature of the program, and each column corresponding to one of the checked statistics. All height data shown in this work was found by using the Maximum value statistic, as we defined the height of a particle by the tallest pixel within the masked area.

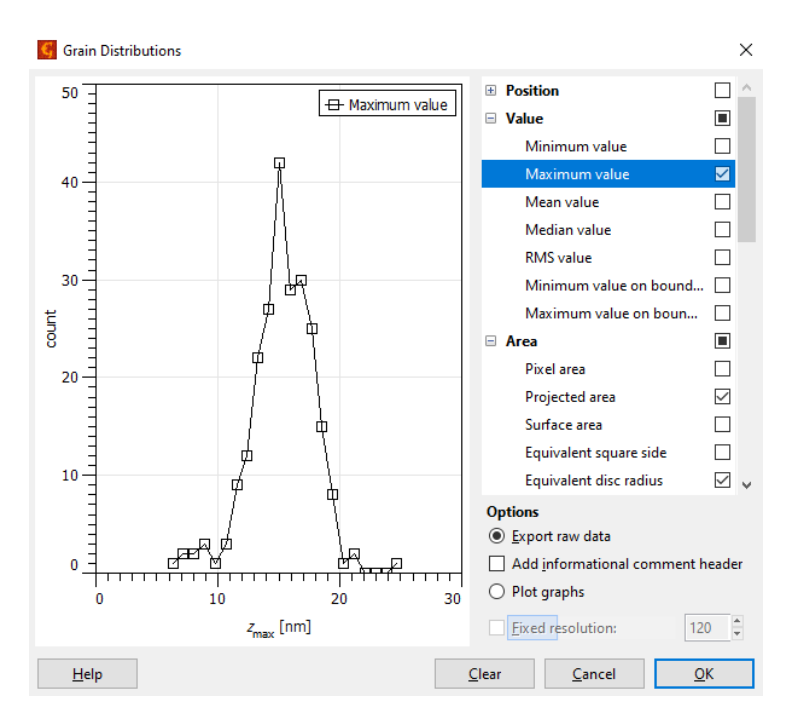


Figure S7: "Distributions of various grain characteristics" window

To analyze the SEM images, it is most common to use ImageJ, and this was used for our study as well. However, it is common to perform operations on SEM images in ImageJ in a similar manner to what was done for the AFM images as described above (ImageJ 1.52a). For our study, this was not possible due to the lack of sufficient contrast in certain images between the background of the substrate and the particles/features of interest. The reasons for how this can occur include imperfect aperture alignment/wobbling correction, imperfect brightness/contrast during image acquisition, poor beam condition and/or poor sample conductivity. In addition, we attributed the poor resolution in some cases to the features themselves being too small, at which point there is not enough volume of material to generate contrast. In these cases, an effort was made to measure as many of the nanoparticles in the SEM images as possible. The use of box plots to present the entire set of measured data as opposed to presenting a single statistical quantity serves to increase the margin for error when making observations.

The following are the steps we took to analyze SEM images using ImageJ.

- 1. Import the scan into ImageJ.
- 2. Use Analyze->Set Scale to convert the pixel units of the image to real distances in nanometers. All images were acquired at the same magnification (300k X, EHT=5 kV, probe current=20 pA), and so the scale was kept consistent for all images. Enter "53.3333" for Distance in pixels, "100" for Known distance, "nm" for Unit of length" and check the Global box. Keep Pixel aspect ratio at 1. This sets the scale as 0.5333 pixels/nm. Using these units, the image's complete size in nm is 1920.00 x 1440.00 nm.

3. Use Analyse->Set Measurements and make sure the Area box is checked. Select the Polygon selections tool (third button from the left). Use this to click around the areas in the image you judge to be a nanoparticle. To finish, select the first point you clicked to close the loop. Then press Ctrl+M or use Analyze->Measure. This opens the measurements window and shows the values for the measured area, as per which boxes were checked in the Set Measurements window. The value presented in this work is Area, measured in nm².

As stated previously, not all SEMs could be measured completely, due to poor contrast between the features of interest and the background. In subsequent section, SEM images will be shown that detail which areas were measured as nanoparticles in order to extract the quantitative data presented in the paper.

<u>Section 2 – AFM and SEM image data and masked and/or measured micrographs for comparison.</u>

In this section, AFM and SEM images available are provided, as well as the versions of the images that show which portions of the images were used to extract the quantitative data presented in the work. We note that not all samples, especially those not discussed in the paper, have both an AFM and SEM image taken for them.

For growths included in the paper, AFM images are provided showing the regions of the AFM which were masked, as well as a corresponding table showing the parameters used in generating the mask. SEM images are provided showing which parts of the image were measured by hand as nanoparticles. For growths not included in the paper, AFM and SEM images are provided if available, along with parameters used in the AFM mask generation. In addition, the justification for why the growth is not included in the main text is provided. For all growths where the AFM was background corrected, and therefore the nanoparticles were masked, height histograms are provided.

Table S1 categorizes all the growths by their sample #, the growth date, the growth parameters used, which sample holder plate was used, doping of the substrate, and whether the growth was included in the work or not. The samples grown before the dashed line in the table were grown prior to our lab shutting down for a period of 2-3 months due to COVID-19.

Growth #	Date grown	t _{Bi} (sec.)	T _{sub} (°C)	Sample plate (Q1, Q2, Q3)	Included in paper (Y/N)
866	01/12/2020	120	250	Q1	N
886	01/28/2020	120	250	Q1	N
898	02/05/2020	20	250	Q3	N
900	02/08/2020	120	275	Q1	N
916	06/26/2020	20	250	Q3	N
917	06/26/2020	60	250	Q2	N
920	07/06/2020	20	275	Q3	N
921	07/06/2020	60	275	Q2	N
946	08/07/2020	20	225	O3	Y

Table S1: Table of parameters for samples grown for this project

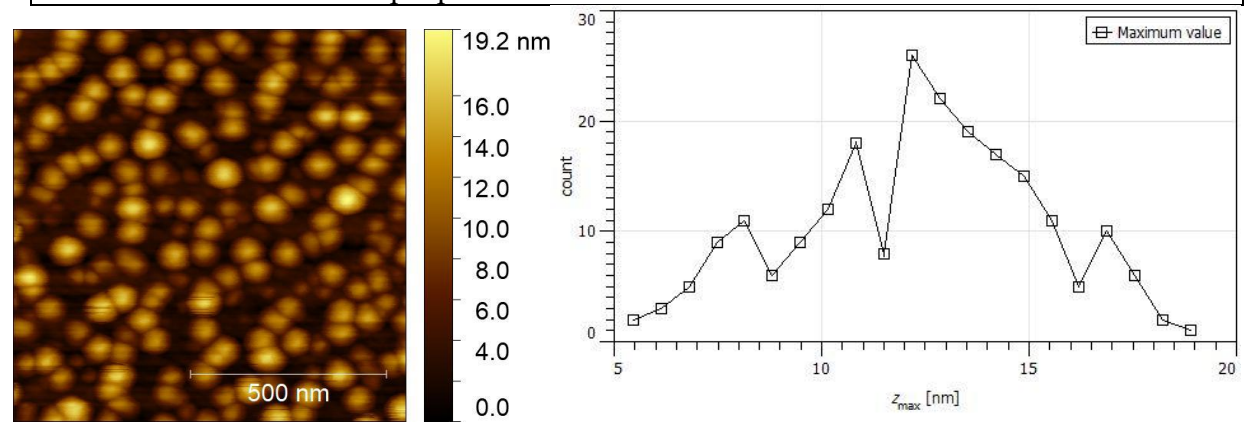
947	08/07/2020	60	225	Q2	Y
950	08/09/2020	20	250	Q2	N
951	08/10/2020	60	250	Q2	N
952	08/10/2020	120	250	Q3	N
986	09/08/2020	$90 (T_{Bi} =$	275	Q3	N
900	09/08/2020	468.7 °C)	213	Q3	19
988	09/11/2020	$30 (T_{Bi} =$	275	Q2	N
700	07/11/2020	500.2 °C)	213	Q ²	
1004	09/25/2020	100	250	Q3	Y
1005	09/25/2020	100	275	Q2	Y
1013	10/01/2020	100	285	Q2	Y
1015	10/03/2020	60	285	Q3	Y
1016	10/03/2020	20	285	Q2	Y
1048	11/14/2020	100	275	Q3	N
		(1820			
		sec. no			
		Bi			
		anneal)			
1049	11/15/2020	60 (1860	275	Q2	N
		sec. no			
		Bi			
		anneal)			
1050	11/15/2020	20 (1900	275	Q3	N
		sec. no			
		Bi			
		anneal)			
1071	12/11/2020	100	350	Q2	N
1072	12/11/2020	60	350	Q3	N
1073	12/12/2020	20	350	Q2	N
1081	12/17/2020	100	325	Q3	Y
1082	12/19/2020	100	250	Q2	N
		(1820			
		sec. no			
		Bi			
		anneal)			
1083	12/19/2020	60 (1820	250	Q3	N
		sec. no			
		Bi			
1000	00/14/2021	anneal)	250	02	37
1098	02/14/2021	40	250	Q2	Y
1099	02/14/2021	80	250	Q3	Y
1109	02/26/2021	20	250	Q3	Y
1110	02/26/2021	60	250	Q2	Y
1122	03/08/2021	60	250	Q3	Y
1124	03/10/2021	60	275	Q3	Y

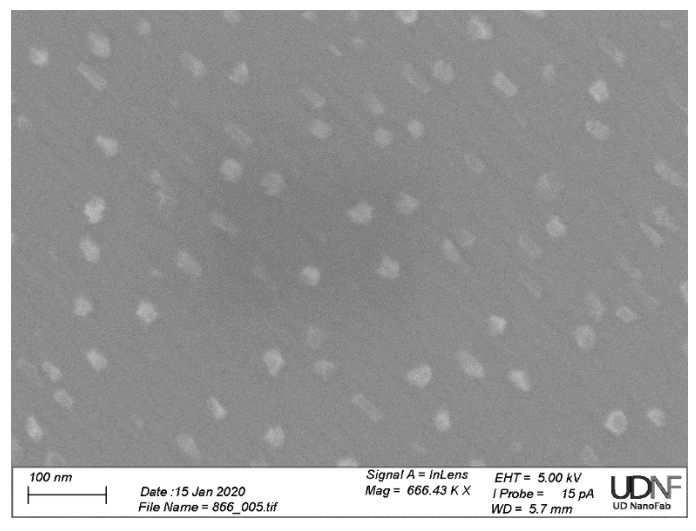
1125	03/11/2021	60	275	Q2	Y
1126	03/11/2021	60	285	Q3	Y
1138	03/23/2021	100	250	Q3	Y

Sample #: 866 $t_{Bi} = 120 \text{ s}, T_{sub} = 250 ^{\circ}\text{C}$	Date: 01/12/2020	Sample plate: Q1
--	------------------	------------------

AFM Segmentation Mask parameters (Gaussian smoothing: 6.16 px, Add gradient: 7.34%, Add curvature: 38.36%, Barrier level: 40.80%, Prefill level: 17.11%, Prefill from minima: 8.91%

Why excluded from paper: Time gap and plate mismatch with comparable growths. Grown before the last time all sample plates were cleaned.

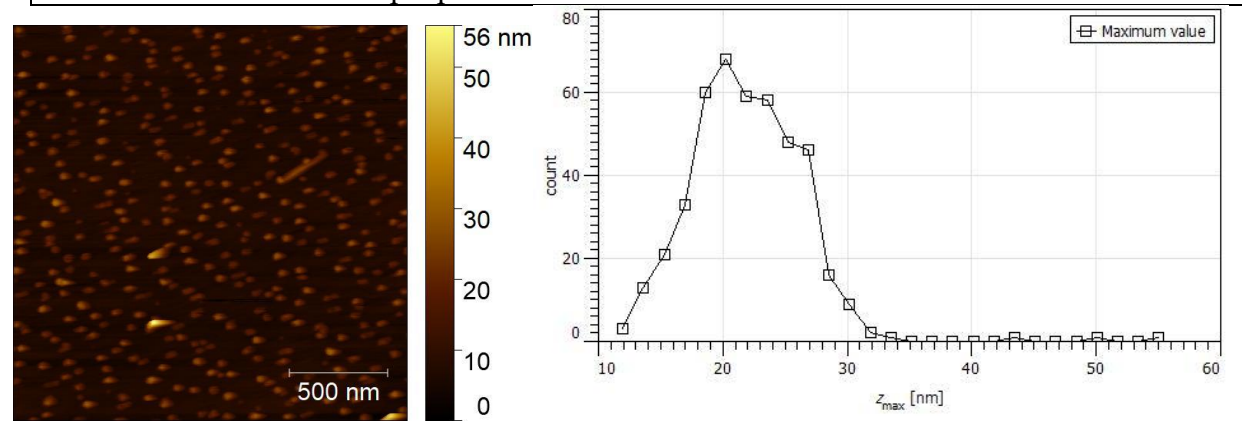


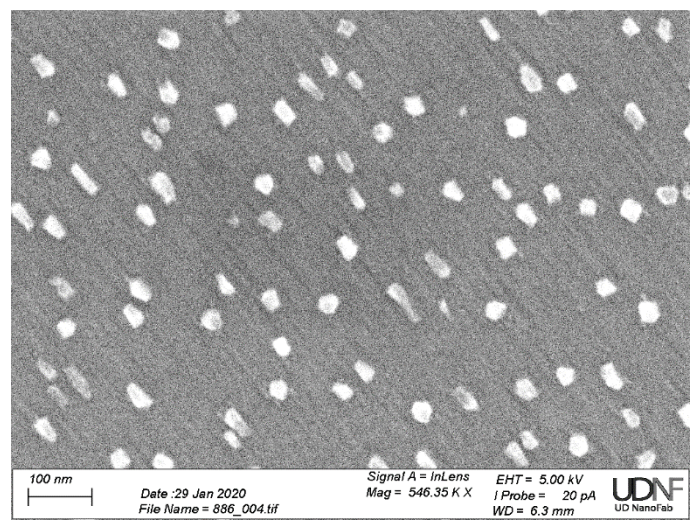


Sample #: 886 | $t_{Bi} = 120 \text{ s}, T_{sub} = 250 \text{ }^{\circ}\text{C}$ | Date: 01/28/2020 | Sample plate: Q1

AFM Segmentation Mask parameters (Gaussian smoothing: 6.16 px, Add gradient: 7.34%, Add curvature: 50.36%, Barrier level: 58.94%, Prefill level: 17.11%, Prefill from minima: 8.91%

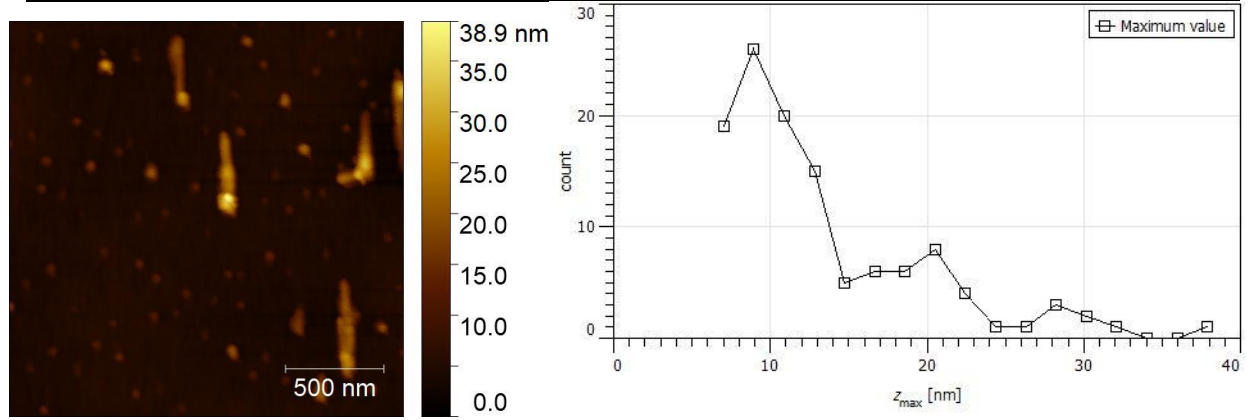
Why excluded from paper: Time gap and plate mismatch with comparable growths. Grown before the last time all sample plates were cleaned.





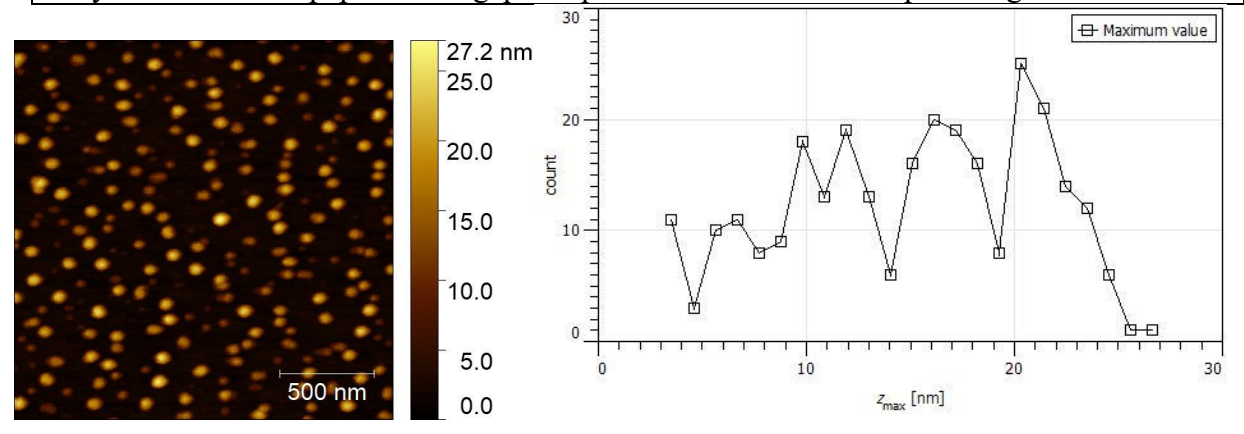
Sample #: 898 | t_{Bi} = 20 s, T_{sub} = 250 °C | Date: 02/05/2020 | Sample plate: Q3 AFM Segmentation Mask parameters (Gaussian smoothing: 5.73 px, Add gradient: 2.81%, Add curvature: 47.65%, Barrier level: 65.04%, Prefill level: 17.11%, Prefill from minima: 8.91%

Why excluded from paper: Time gap with comparable growths.



Sample #: 900 $t_{Bi} = 120 \text{ s}, T_{sub} = 275 \text{ °C}$ Date: 02/08/2020 Sample plate: Q1

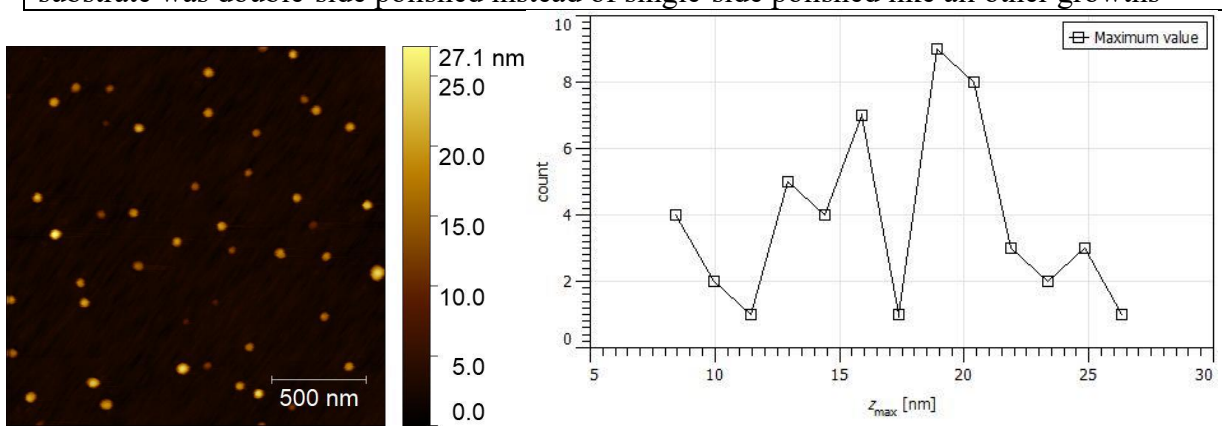
AFM Segmentation Mask parameters (Gaussian smoothing: 5.73 px, Add gradient: 2.81%, Add curvature: 37.57%, Barrier level: 65.04%, Prefill level: 17.11%, Prefill from minima: 8.91%

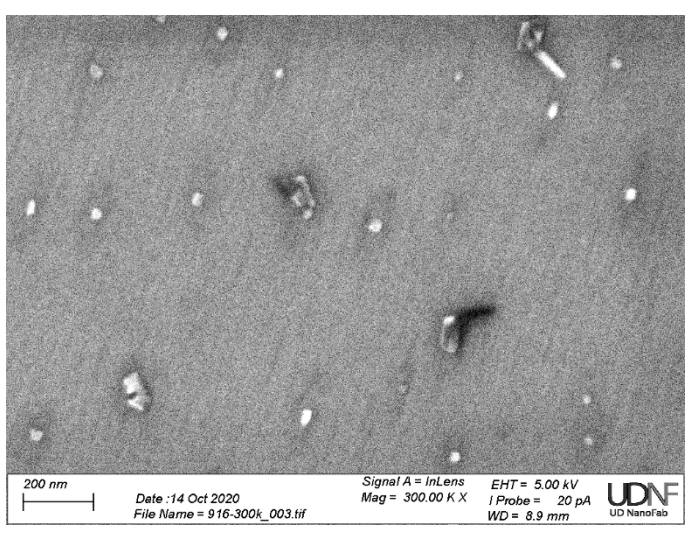


Sample #: 916 | $t_{Bi} = 20 \text{ s}, T_{sub} = 250 \text{ °C}$ | Date: 06/26/2020 | Sample plate: Q3

AFM Segmentation Mask parameters (Gaussian smoothing: 2.00 px, Add gradient: 5.10%, Add curvature: 31.50%, Barrier level: 58.94%, Prefill level: 27.31%, Prefill from minima: 16.52%

Why excluded from paper: Time gap and plate mismatch with comparable growths, substrate was double-side polished instead of single-side polished like all other growths

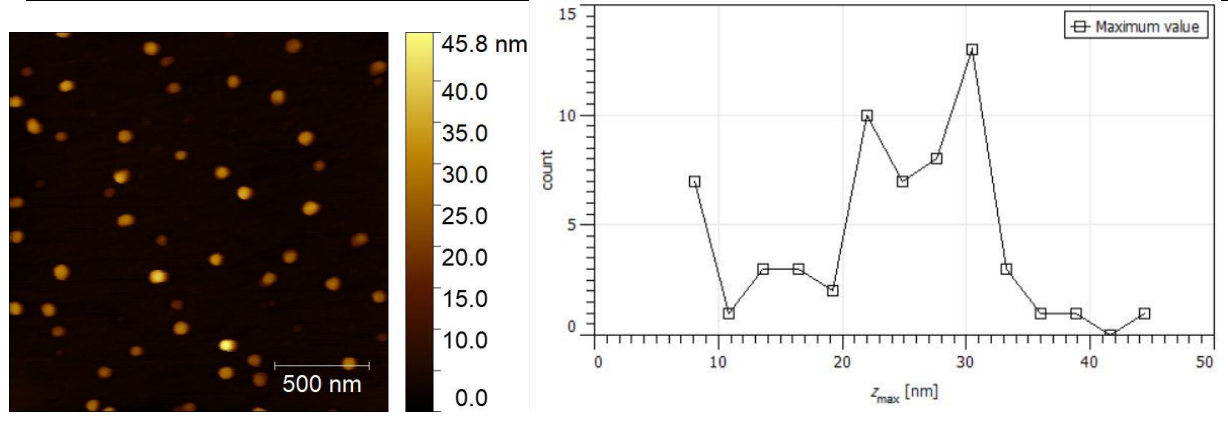


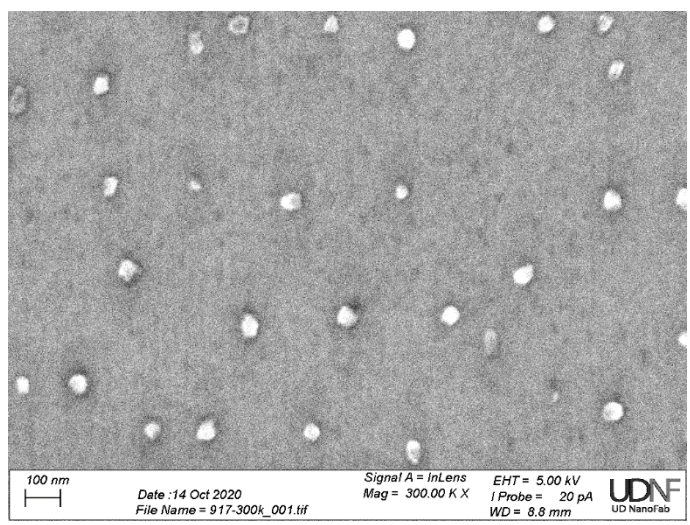


Sample #: 917 $t_{Bi} = 60 \text{ s}, T_{sub} = 250 \text{ °C}$ Date: 06/26/2020 Sample plate: Q2

AFM Segmentation Mask parameters (Gaussian smoothing: 4.82 px, Add gradient: 5.10%, Add curvature: 31.50%, Barrier level: 65.93%, Prefill level: 27.31%, Prefill from minima: 16.52%

Why excluded from paper: Time gap and/or plate mismatch with comparable growths, substrate was double-side polished instead of single-side polished like all other growths

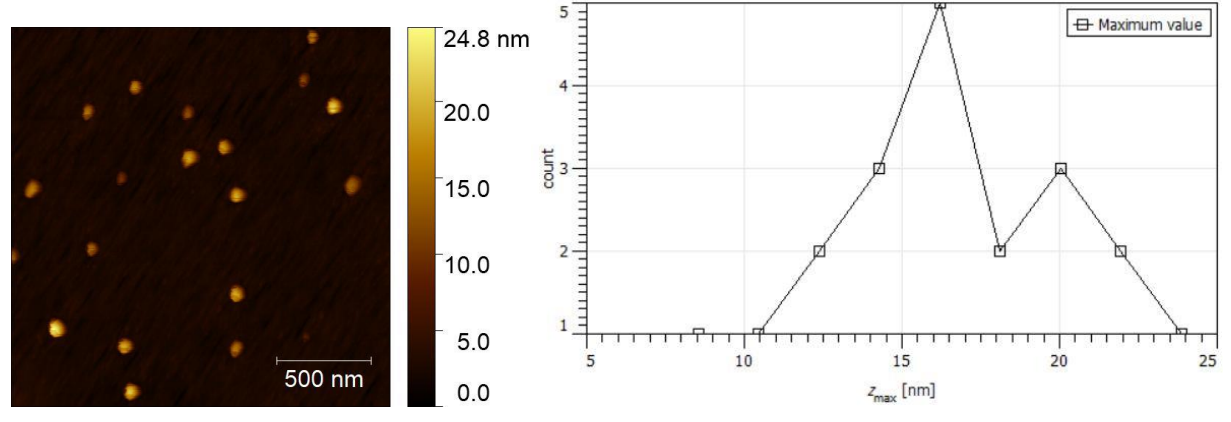


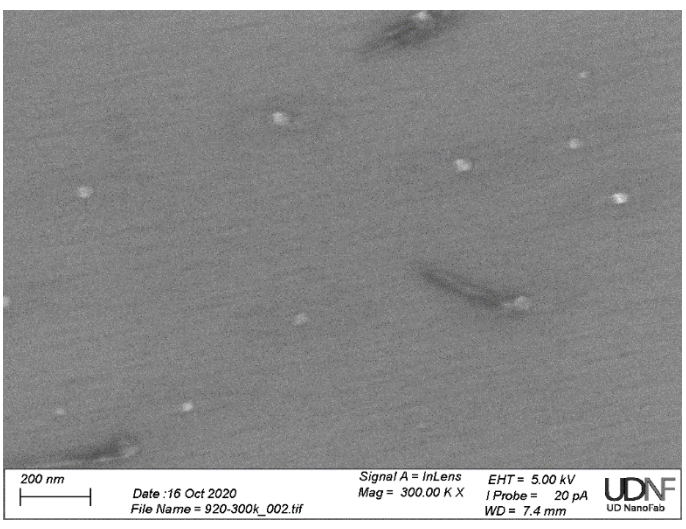


Sample #: 920 | $t_{Bi} = 20 \text{ s}, T_{sub} = 275 \text{ °C}$ | Date: 07/06/2020 | Sample plate: Q3

AFM Segmentation Mask parameters (Gaussian smoothing: 4.56 px, Add gradient: 5.10%, Add curvature: 31.50%, Barrier level: 58.94%, Prefill level: 27.31%, Prefill from minima: 16.52%

Why excluded from paper: Time gap and/or plate mismatch with comparable growths, substrate was double-side polished instead of single-side polished like all other growths

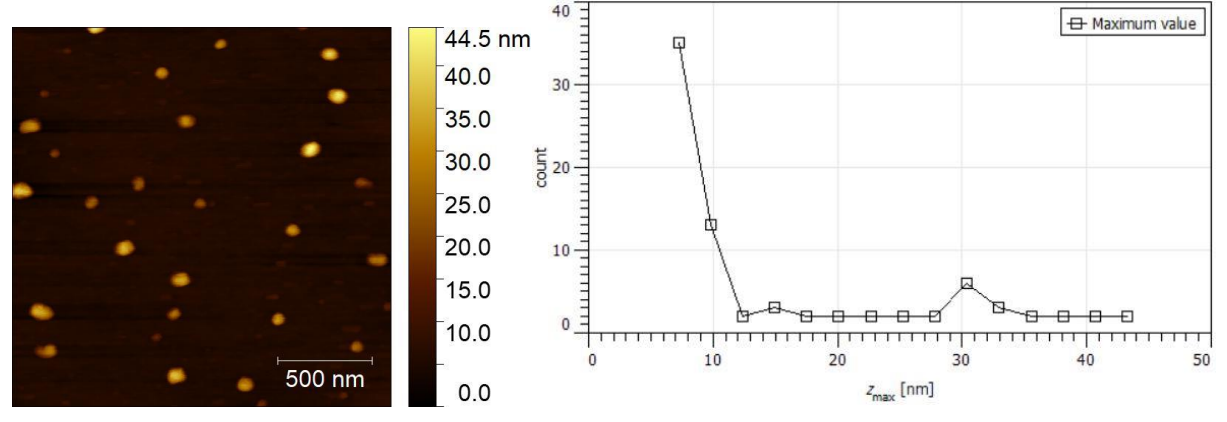


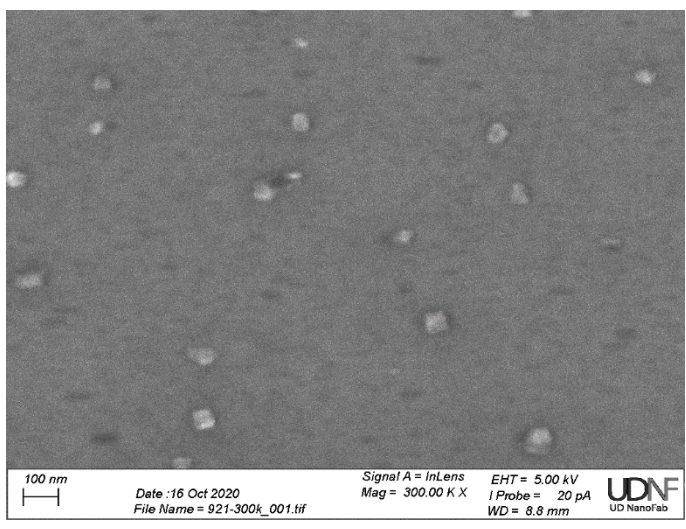


Sample #: 921 $t_{Bi} = 60 \text{ s}, T_{sub} = 275 \text{ °C}$ Date: 07/06/2020 Sample plate: Q2

AFM Segmentation Mask parameters (Gaussian smoothing: 5.33 px, Add gradient: 8.81%, Add curvature: 55.50%, Barrier level: 57.96%, Prefill level: 27.31%, Prefill from minima: 16.52%

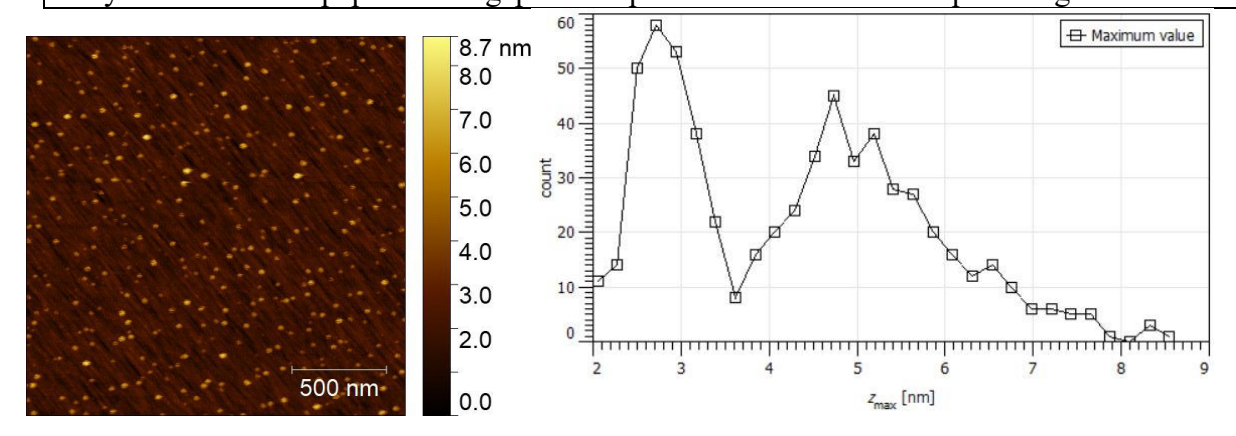
Why excluded from paper: Time gap and/or plate mismatch with comparable growths, substrate was double-side polished instead of single-side polished like all other growths





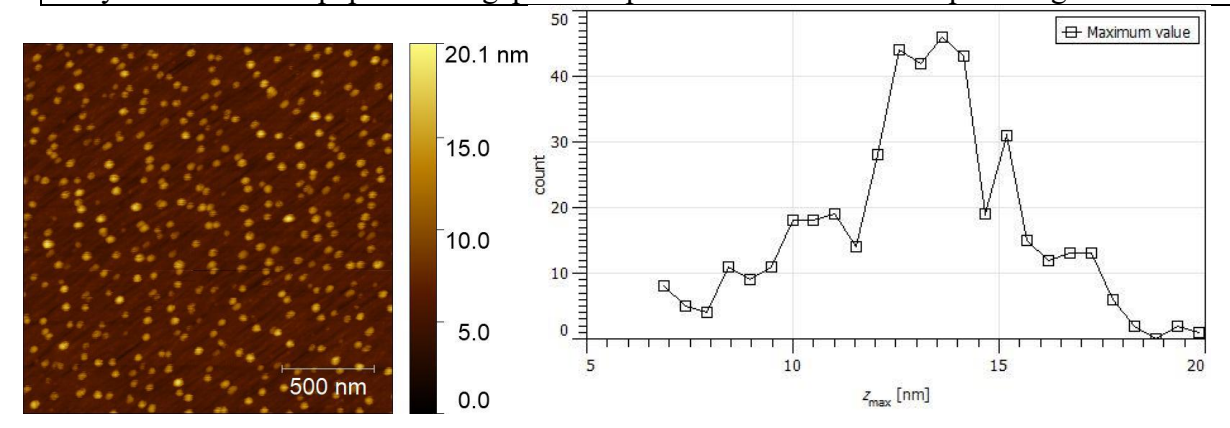
Sample #: 950	$t_{Bi} = 20 \text{ s}, T_{sub} = 250 ^{\circ}\text{C} \text{ (Se)}$	Date: 08/09/2020	Sample plate: Q2
	closed at $T_{\text{sub}} = 180 ^{\circ}\text{C}$		

AFM Segmentation Mask parameters (1 scar removal, Gaussian smoothing: 6.30 px, Add gradient: 8.81%, Add curvature: 60.94%, Barrier level: 47.65%, Prefill level: 27.31%, Prefill from minima: 16.52%



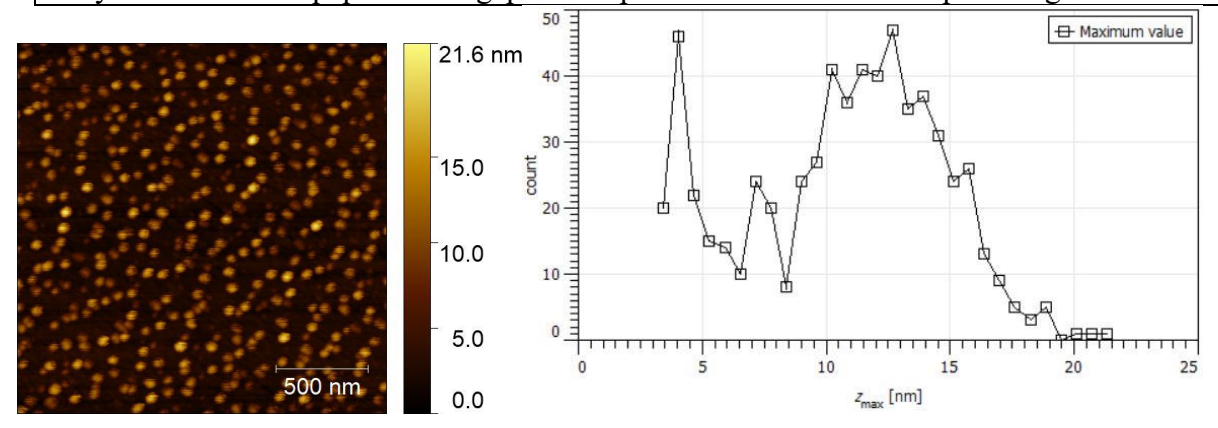
Sample #: 951	$t_{Bi} = 60 \text{ s}, T_{sub} = 250 ^{\circ}\text{C} \text{ (Se)}$	Date: 08/10/2020	Sample plate: Q2
	closed at $T_{\text{sub}} = 180 ^{\circ}\text{C}$		

AFM Segmentation Mask parameters (1 scar removal, Gaussian smoothing: 4.20 px, Add gradient: 9.59%, Add curvature: 40.80%, Barrier level: 53.15%, Prefill level: 16.52%, Prefill from minima: 7.70%



Sample #: 952	$t_{Bi} = 120 \text{ s}, T_{sub} = 250 \text{ C} \text{ (Se)}$	Date: 08/10/2020	Sample plate: Q3
	closed at $T_{\text{sub}} = 180 \text{ C}$		

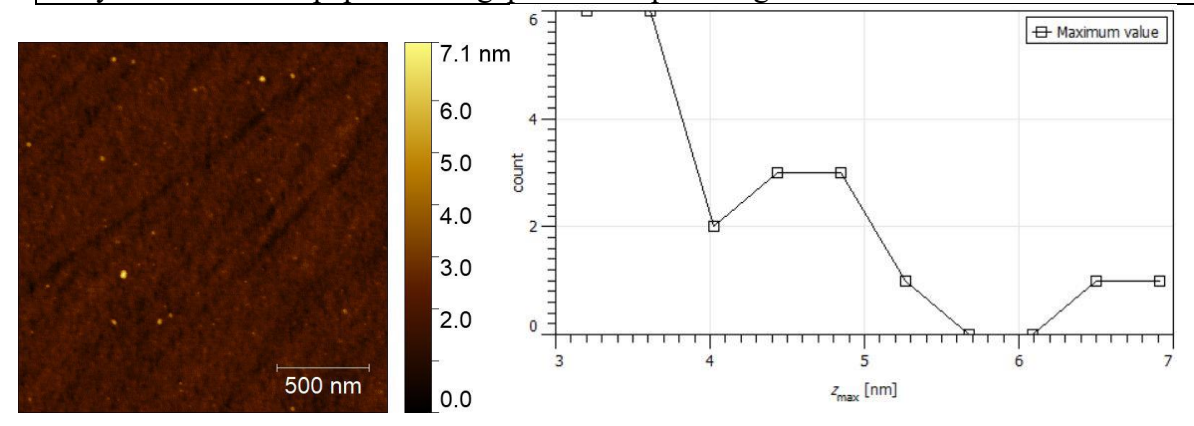
AFM Segmentation Mask parameters (Gaussian smoothing: 4.20 px, Add gradient: 9.59%, Add curvature: 40.80%, Barrier level: 53.15%, Prefill level: 16.52%, Prefill from minima: 7.70%



Sample #: 986	$t_{Bi} = 90 \text{ s}, T_{sub} = 275 ^{\circ}\text{C} (T_{Bi})$	Date: 09/08/2020	Sample plate: Q3
	$= 468.7 {}^{\circ}\text{C}$		

AFM Segmentation Mask parameters (Gaussian smoothing: 1.47 px, Add gradient: 2.81%, Add curvature: 46.77%, Barrier level: 25.98%, Prefill level: 17.11%, Prefill from minima: 8.91%

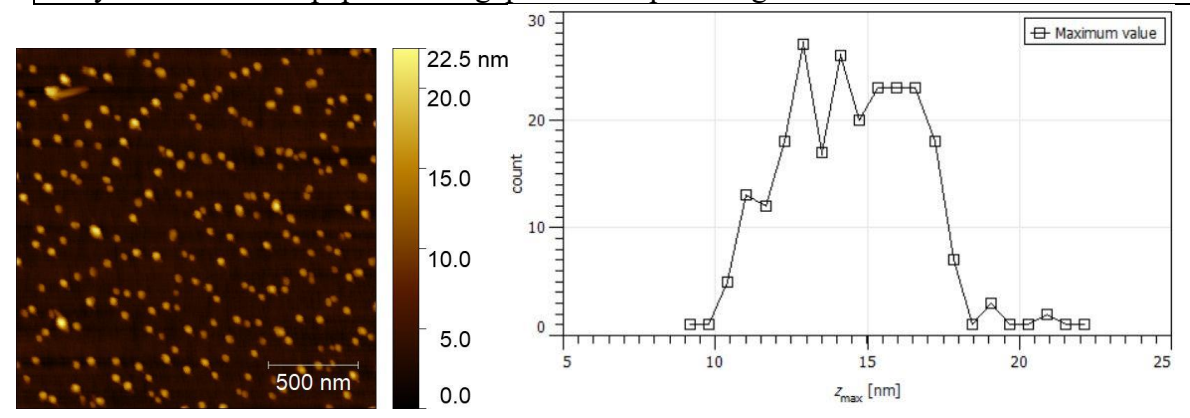
Why excluded from paper: Time gap with comparable growths.



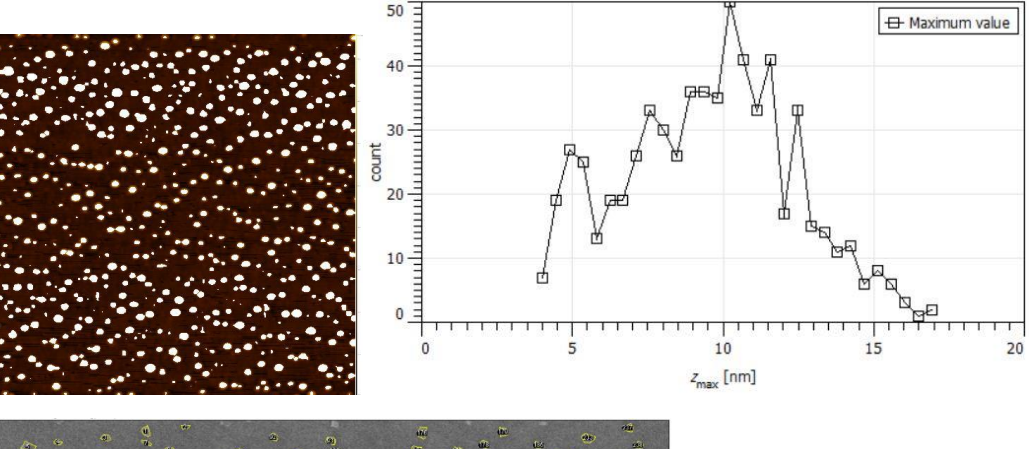
Sample #: 988	$t_{Bi} = 30 \text{ s}, T_{sub} = 275 ^{\circ}\text{C} (T_{Bi})$	Date: 09/11/2020	Sample plate: Q2
	$= 500.2 {}^{\circ}\text{C}$		

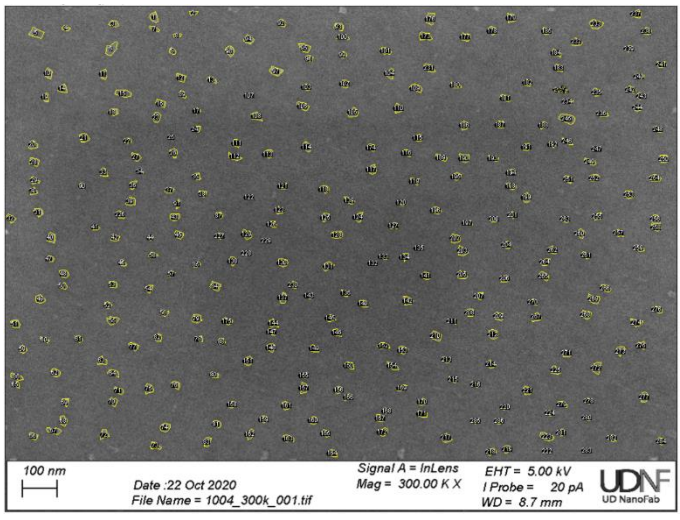
AFM Segmentation Mask parameters (Gaussian smoothing: 5.73 px, Add gradient: 11.25%, Add curvature: 57.96%, Barrier level: 51.28%, Prefill level: 17.11%, Prefill from minima: 8.91%

Why excluded from paper: Time gap with comparable growths.

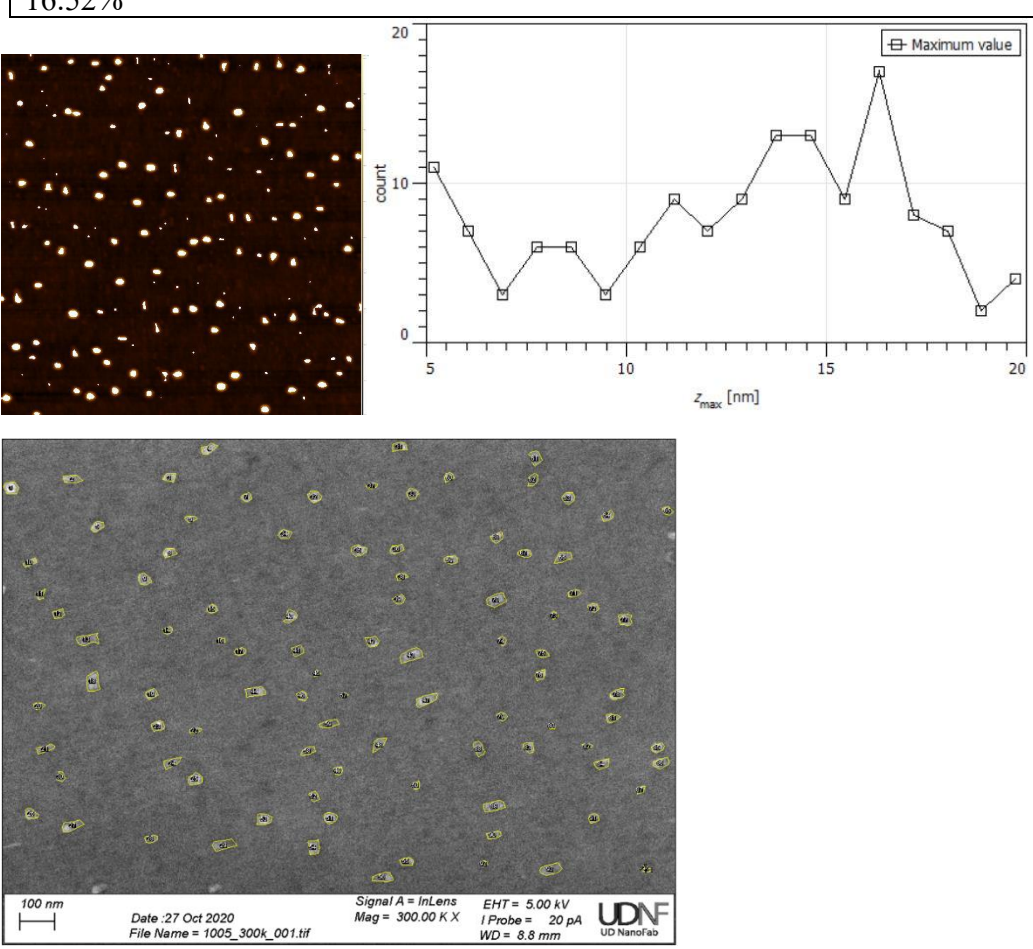


Sample #: 1004 | t_{Bi} = 100 s, T_{sub} = 250 C | Date: 09/25/2020 | Sample plate: Q3 AFM Segmentation Mask parameters (Gaussian smoothing: 4.56 px, Add gradient: 6.33%, Add curvature: 49.45%, Barrier level: 53.15%, Prefill level: 21.58%, Prefill from minima: 3.26%

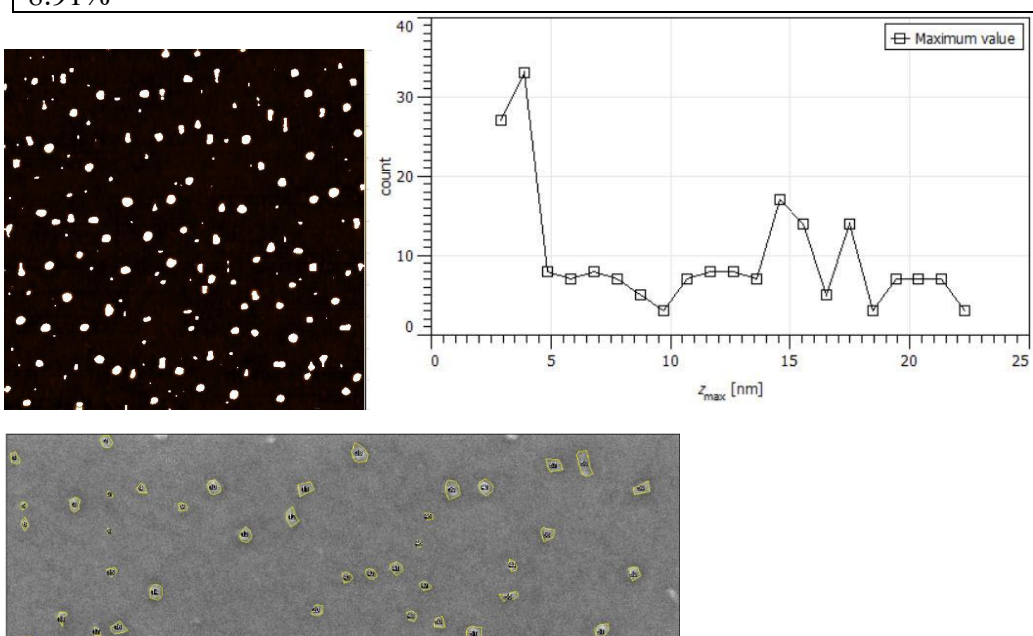




Sample #: 1005 | $t_{Bi} = 100$ s, $T_{sub} = 275$ C | Date: 09/25/2020 | Sample plate: Q2 AFM Segmentation Mask parameters (Gaussian smoothing: 5.46 px, Add gradient: 8.81%, Add curvature: 62.38%, Barrier level: 58.01%, Prefill level: 27.31%, Prefill from minima: 16.52%

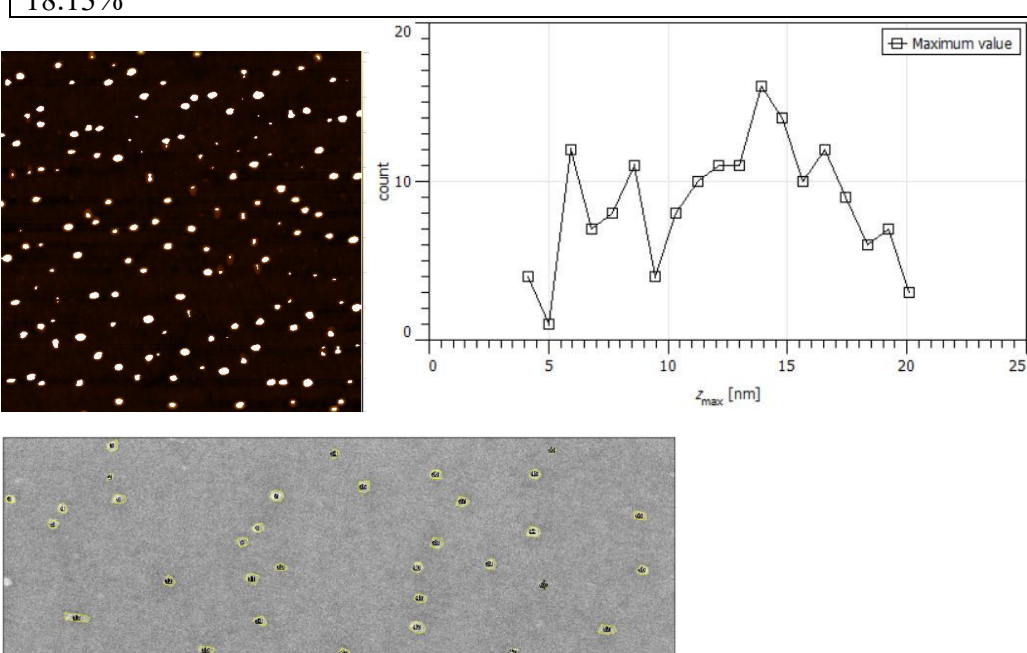


Sample #: 1013 | $t_{Bi} = 100$ s, $T_{sub} = 285$ C | Date: 10/01/2020 | Sample plate: Q2 AFM Segmentation Mask parameters (Gaussian smoothing: 5.06 px, Add gradient: 9.91%, Add curvature: 53.15%, Barrier level: 64.00%, Prefill level: 17.11%, Prefill from minima: 8.91%



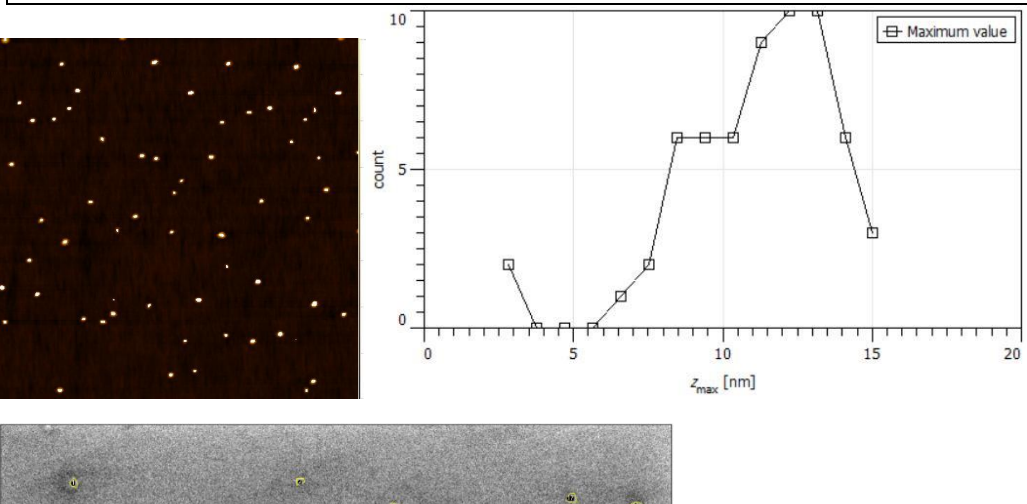
Signal A = InLens Mag = 300.00 K X

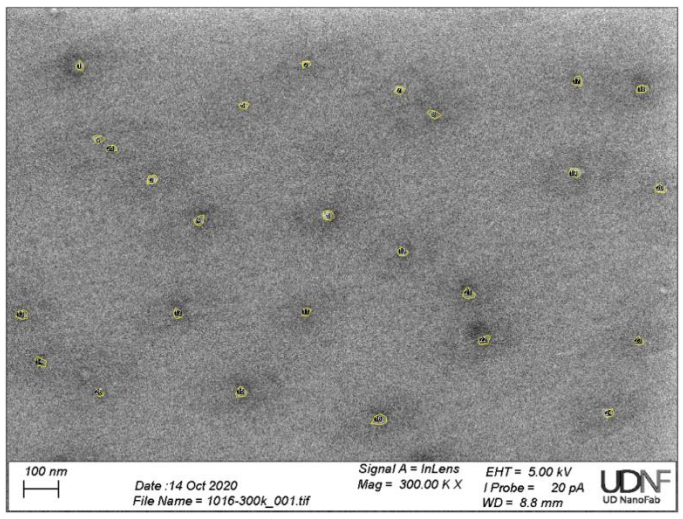
Date :16 Oct 2020 File Name = 1013-300k_003.tif EHT = 5.00 kV I Probe = 20 pA WD = 8.7 mm Sample #: 1015 | $t_{Bi} = 60$ s, $T_{sub} = 285$ C | Date: 10/03/2020 | Sample plate: Q3 AFM Segmentation Mask parameters (Gaussian smoothing: 2.80 px, Add gradient: 13.05%, Add curvature: 29.37%, Barrier level: 55.05%, Prefill level: 36.00%, Prefill from minima: 18.13%



EHT = 5.00 kV I Probe = 20 pA WD = 8.9 mm

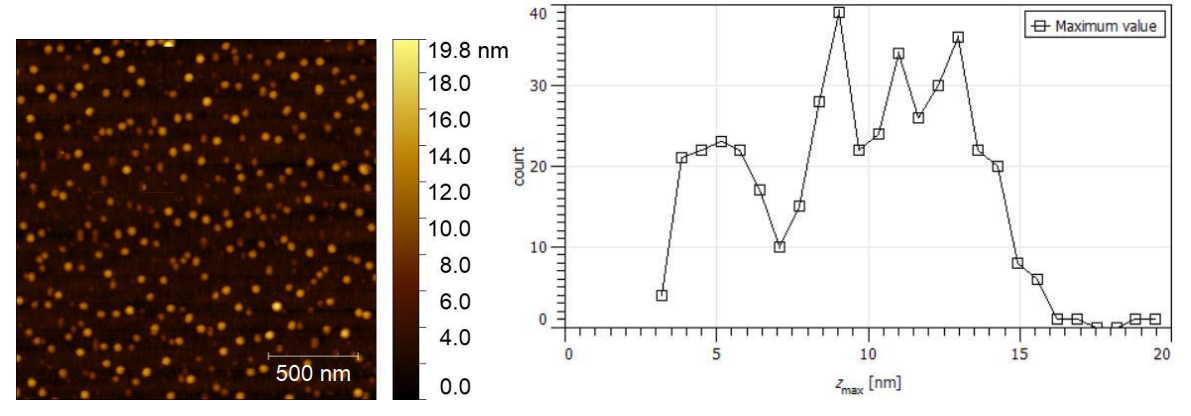
Date :14 Oct 2020 File Name = 1015-300k_002.tif Sample #: 1016 | t_{Bi} = 20 s, T_{sub} = 285 C | Date: 10/03/2020 | Sample plate: Q2 AFM Segmentation Mask parameters (Gaussian smoothing: 5.77 px, Add gradient: 9.99%, Add curvature: 55.37%, Barrier level: 51.98%, Prefill level: 17.11%, Prefill from minima: 8.91%

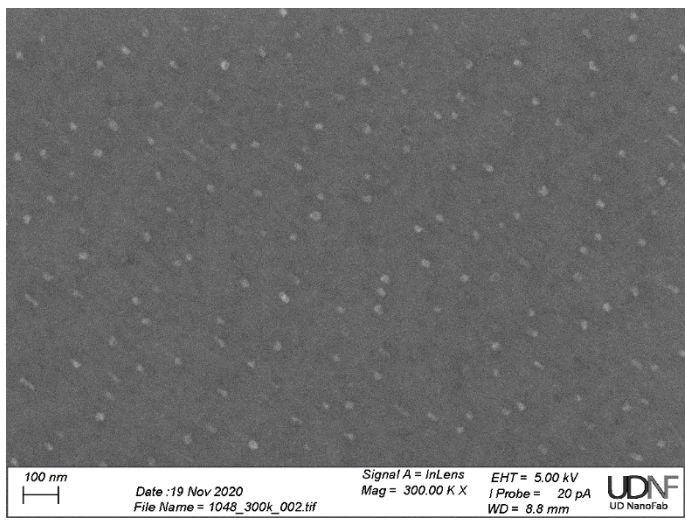




Sample #: 1048	$t_{Bi} = 100 \text{ s} (1820 \text{ sec. no Bi})$	Date: 11/14/2020	Sample plate: Q3
	anneal), $T_{\text{sub}} = 275 ^{\circ}\text{C}$		

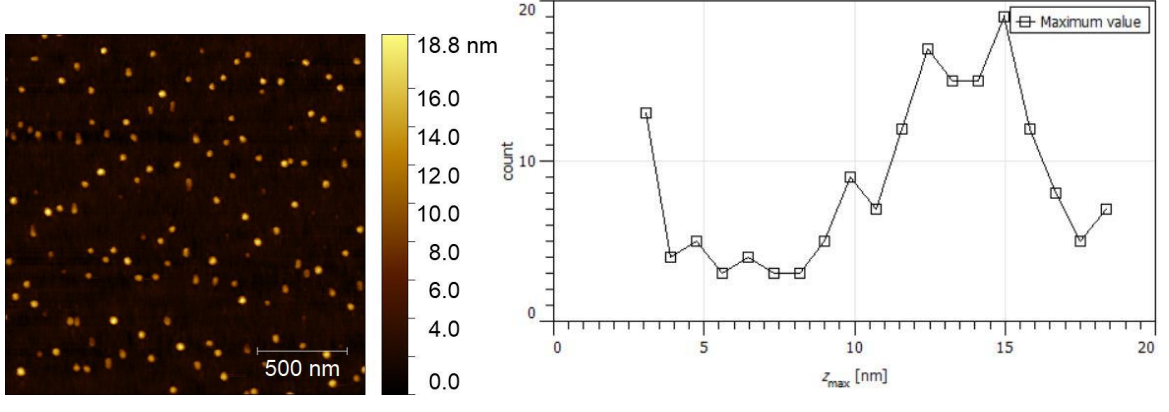
AFM Segmentation Mask parameters (Gaussian smoothing: 3.10 px, Add gradient: 7.34%, Add curvature: 61.95%, Barrier level: 36.00%, Prefill level: 17.11%, Prefill from minima: 8.91%

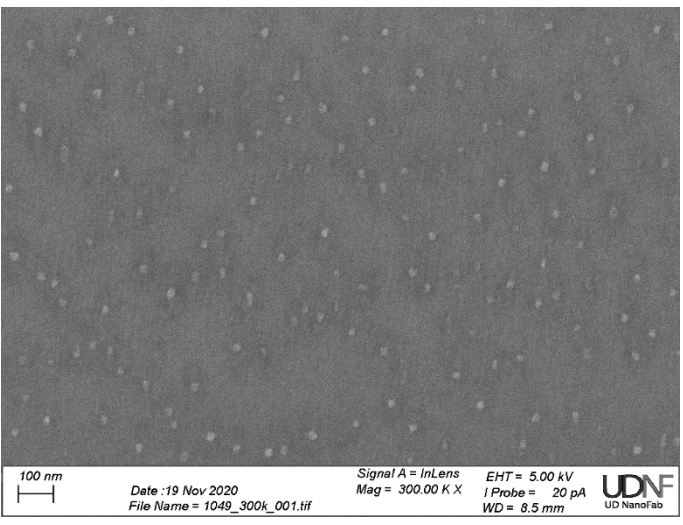




Sample #: 1049	$t_{Bi} = 60 \text{ s} (1860 \text{ sec. no Bi})$	Date: 11/15/2020	Sample plate: Q2
	anneal), $T_{\text{sub}} = 275 ^{\circ}\text{C}$		

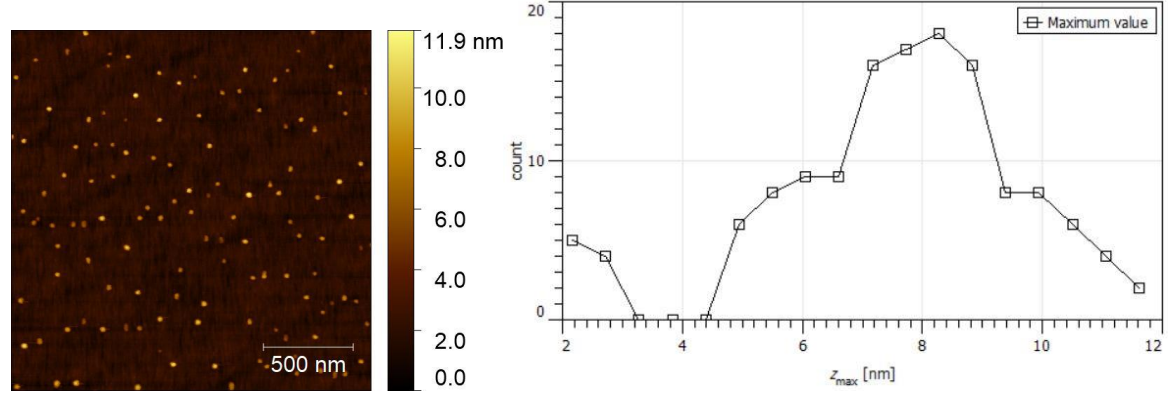
AFM Segmentation Mask parameters (Gaussian smoothing: 4.44 px, Add gradient: 9.59%, Add curvature: 40.80%, Barrier level: 56.98%, Prefill level: 16.52%, Prefill from minima: 7.70%

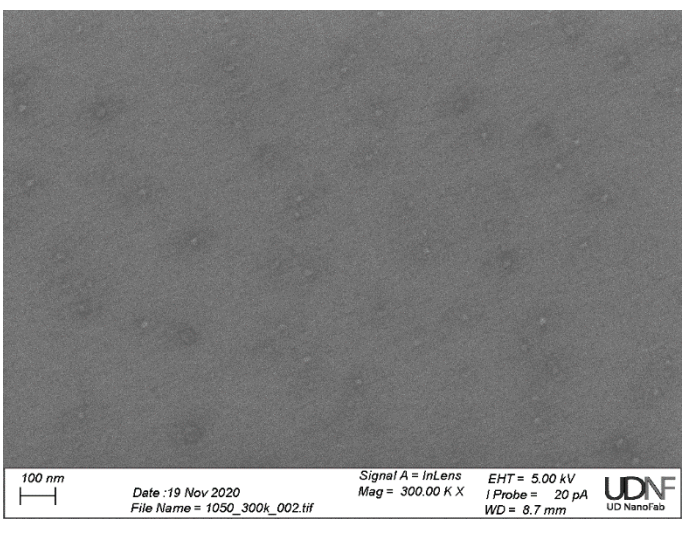




Sample #: 1050	$t_{Bi} = 20 \text{ s} (1900 \text{ sec. no Bi})$	Date: 11/15/2020	Sample plate: Q3
	anneal), $T_{\text{sub}} = 275 ^{\circ}\text{C}$		

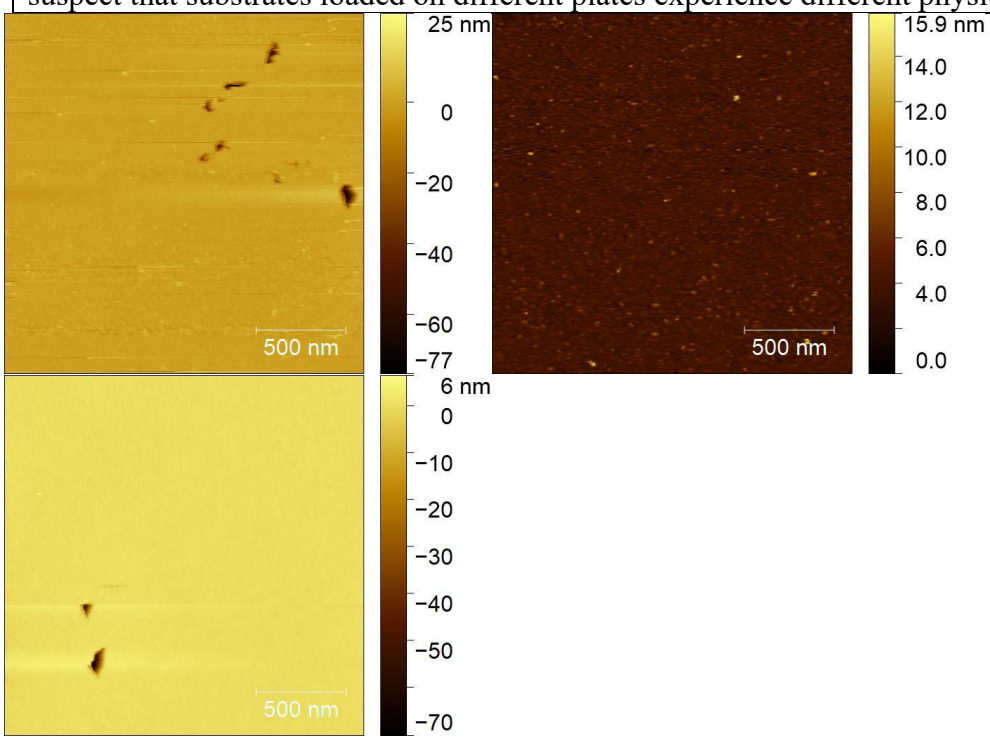
AFM Segmentation Mask parameters (Gaussian smoothing: 4.32 px, Add gradient: 9.59%, Add curvature: 59.94%, Barrier level: 31.50%, Prefill level: 16.52%, Prefill from minima: 7.70%





Sample #: 1071	$t_{Bi} = 100 \text{ s}, T_{sub} = 350 ^{\circ}\text{C}$	Date: 12/11/2020	Sample plate: Q2
Sample #: 1072	$t_{Bi} = 60 \text{ s}, T_{sub} = 350 ^{\circ}\text{C}$	Date: 12/11/2020	Sample plate: Q3
Sample #: 1073	$t_{\rm Bi} = 20 \text{ s}, T_{\rm sub} = 350 ^{\rm o}{\rm C}$	Date: 12/12/2020	Sample plate: Q2

Why excluded from paper: 1071 and 1073 exhibited pitting in AFM, suggesting that for this substrate temperature, the selenium overpressure was insufficient to prevent arsenic degassing from the GaAs substrate. 1072 did not exhibit this pitting, and this is attributed to the fact that it was grown on a different sample plate. As discussed in the main text, we suspect that substrates loaded on different plates experience different physical temperatures.

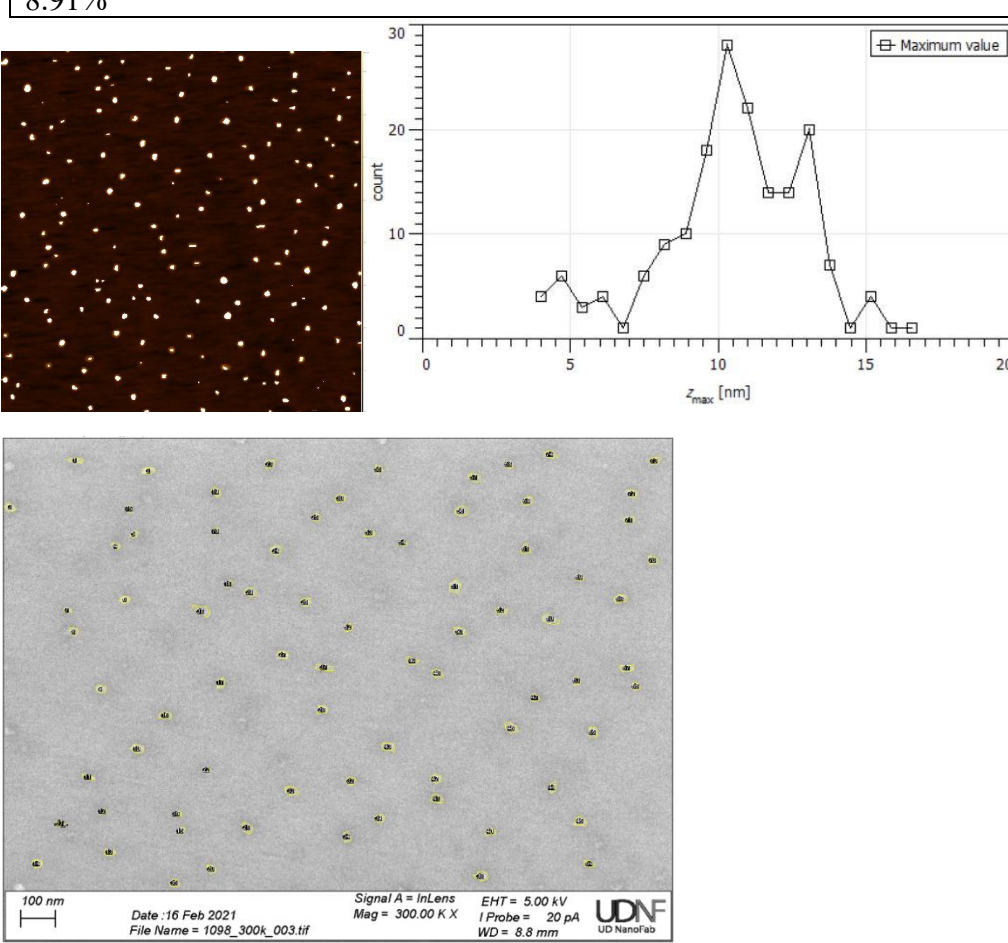


Sample #: 1082	$t_{Bi} = 100 \text{ s} (1820 \text{ sec. no Bi})$	Date: 12/19/2020	Sample plate: Q2
	anneal), $T_{\text{sub}} = 250 ^{\circ}\text{C}$		

Why excluded from paper: Time gap and/or plate mismatch with comparable growths. AFM data not provided due to "kink" in the data which could not be resolved using the prescribed procedure.

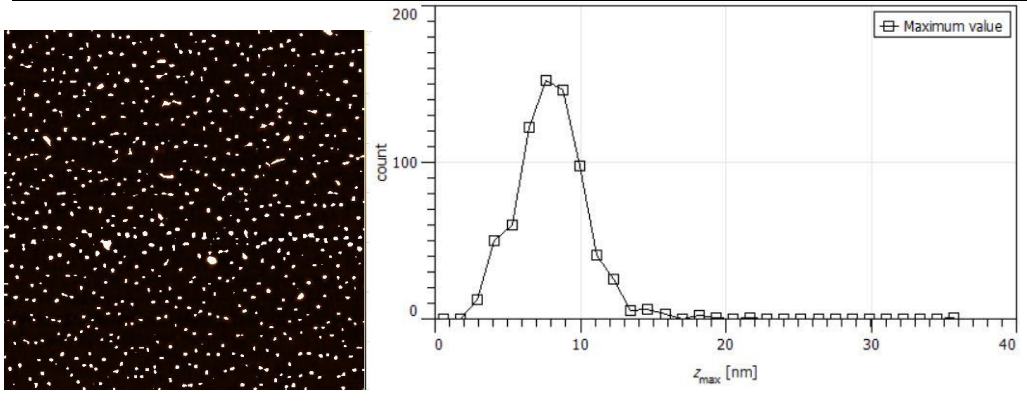
Sample #: 1083	$t_{Bi} = 60 \text{ s} (1860 \text{ sec. no Bi})$	Date: 12/19/2020	Sample plate: Q3			
	anneal), $T_{\text{sub}} = 250 ^{\circ}\text{C}$					
Why excluded from paper: Time gap and/or plate mismatch with comparable growths.						
Complete AFM scan was not able to be obtained due to errors in scanning.						

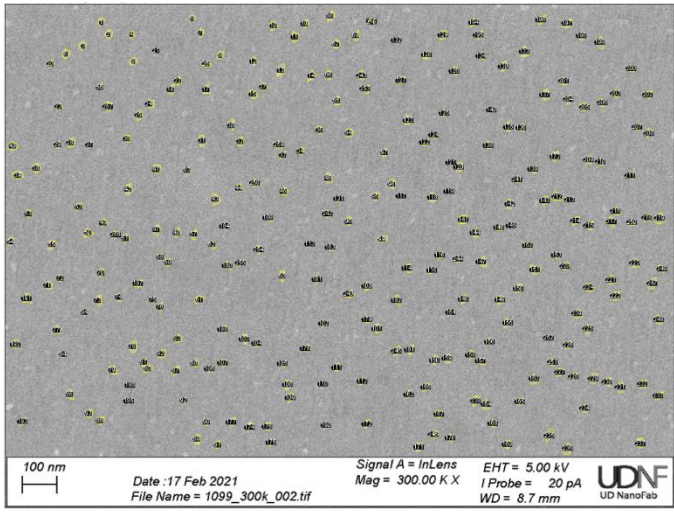
Sample #: 1098 $t_{Bi} = 40 \text{ s}, T_{sub} = 250 \text{ }^{\circ}\text{C}$ Date: 02/14/2021 Sample plate: Q2 AFM Segmentation Mask parameters (Gaussian smoothing: 5.77 px, Add gradient: 9.99%, Add curvature: 55.37%, Barrier level: 51.98%, Prefill level: 17.11%, Prefill from minima: 8.91%



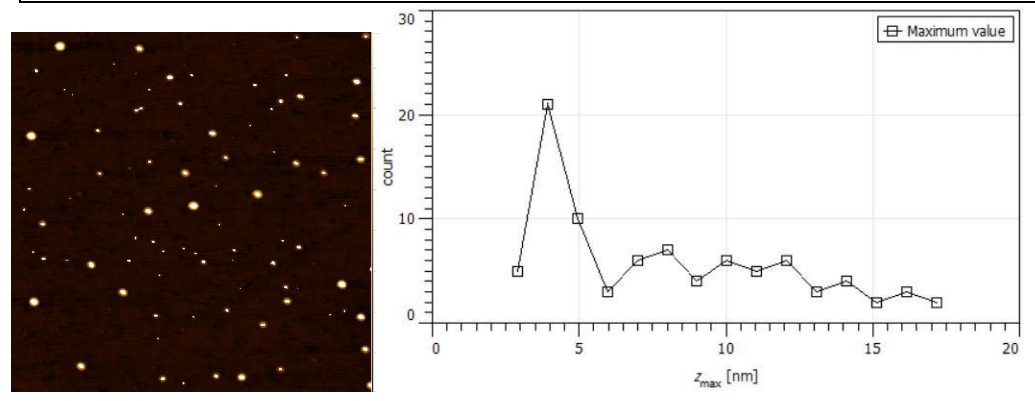
Date :16 Feb 2021 File Name = 1098_300k_003.tif

Sample #: 1099 $t_{Bi} = 80 \text{ s}$, $T_{sub} = 250 \text{ °C}$ Date: 02/14/2021 Sample plate: Q3 AFM Segmentation Mask parameters (Gaussian smoothing: 5.22 px, Add gradient: 14.00%, Add curvature: 69.27%, Barrier level: 64.22%, Prefill level: 24.68%, Prefill from minima: 14.49%

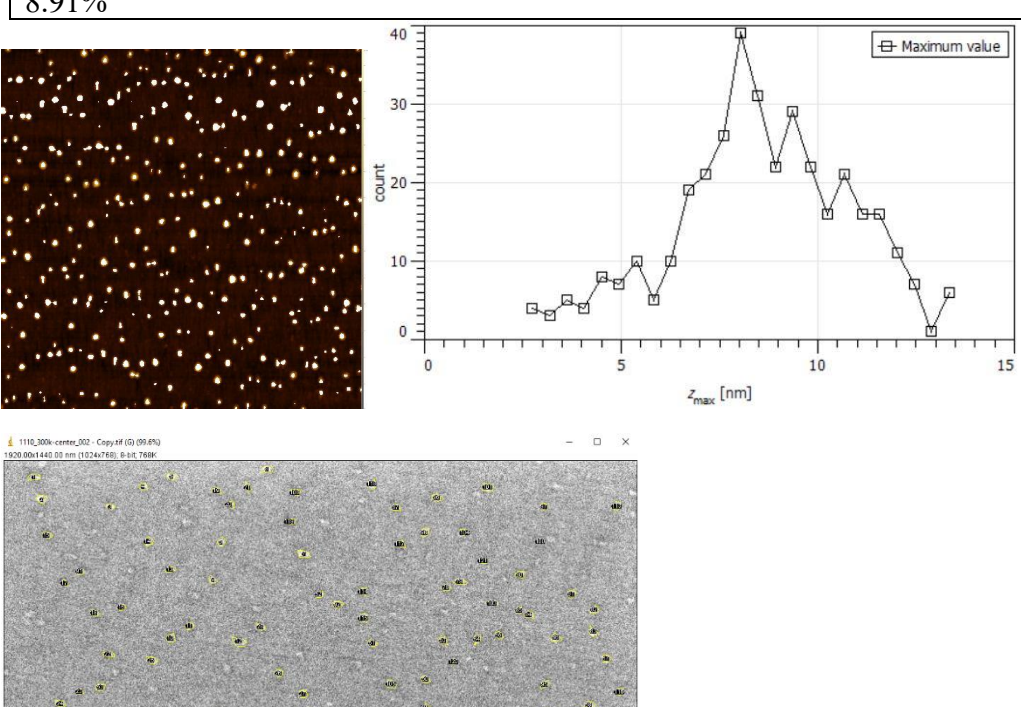




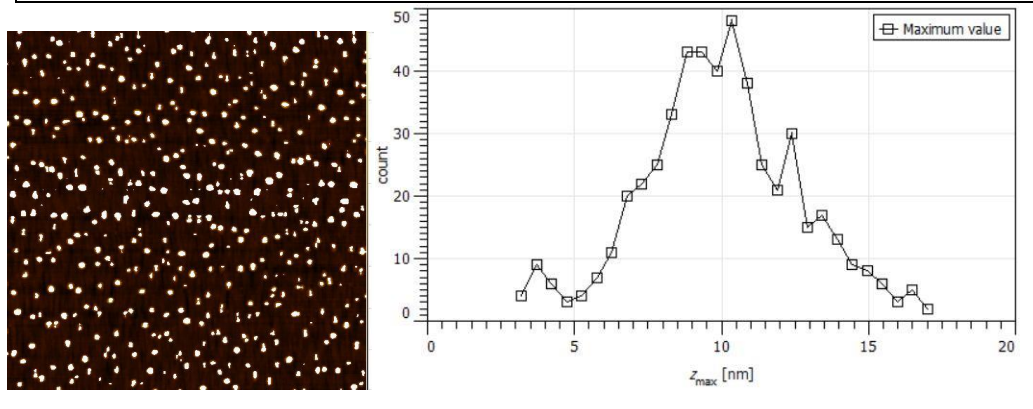
Sample #: 1109 | t_{Bi} = 20 s, T_{sub} = 250 °C | Date: 02/26/2021 | Sample plate: Q3 AFM Segmentation Mask parameters (Gaussian smoothing: 5.93 px, Add gradient: 8.60%, Add curvature: 64.17%, Barrier level: 50.87%, Prefill level: 17.11%, Prefill from minima: 8.91%

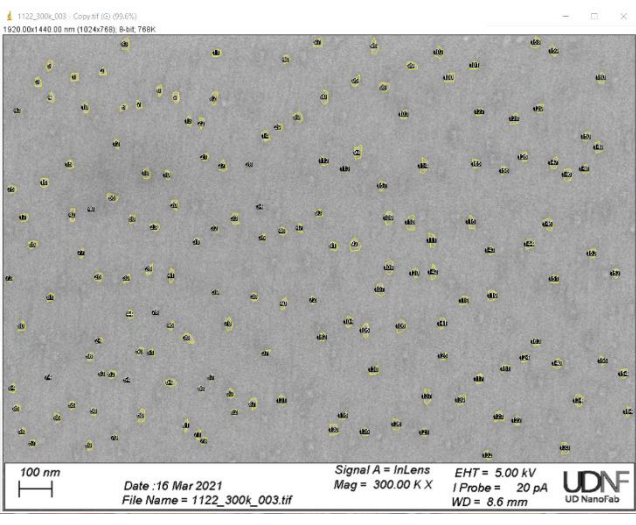


Sample #: 1110 | $t_{Bi} = 60 \text{ s}$, $T_{sub} = 250 \text{ °C}$ | Date: 02/26/2021 | Sample plate: Q2 AFM Segmentation Mask parameters (Gaussian smoothing: 5.77 px, Add gradient: 9.99%, Add curvature: 55.37%, Barrier level: 48.94%, Prefill level: 17.11%, Prefill from minima: 8.91%

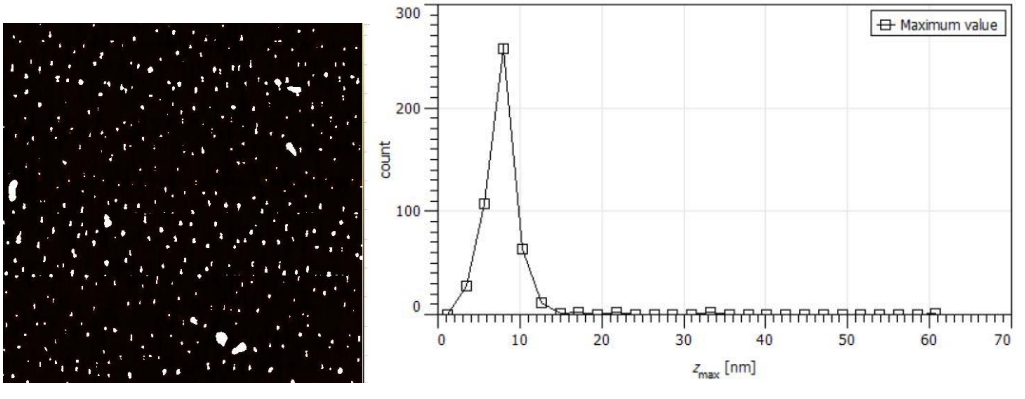


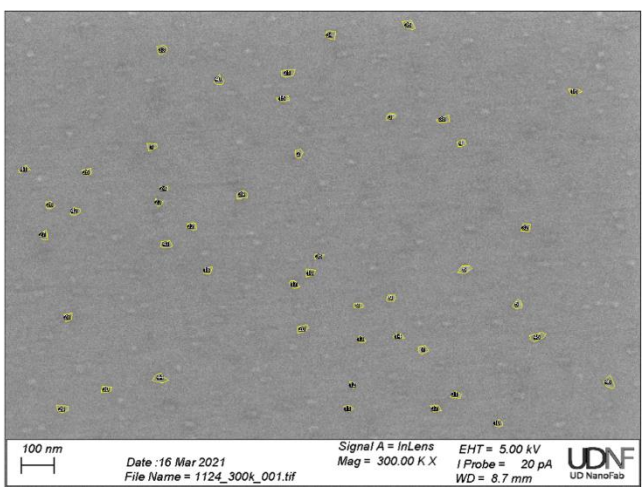
EHT = 5.00 kV I Probe = 20 pA WD = 8.8 mm Sample #: 1122 | t_{Bi} = 60 s, T_{sub} = 250 °C | Date: 03/08/2021 | Sample plate: Q3 AFM Segmentation Mask parameters (Gaussian smoothing: 3.59 px, Add gradient: 9.99%, Add curvature: 49.45%, Barrier level: 53.57%, Prefill level: 17.11%, Prefill from minima: 8.91%



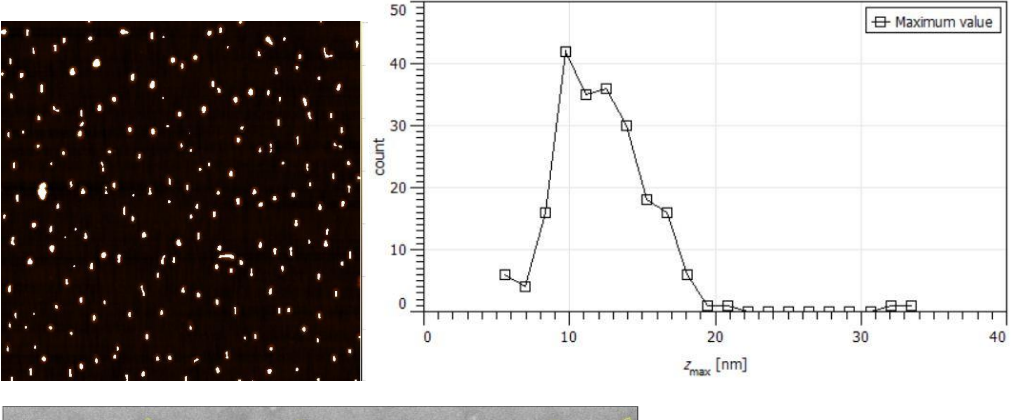


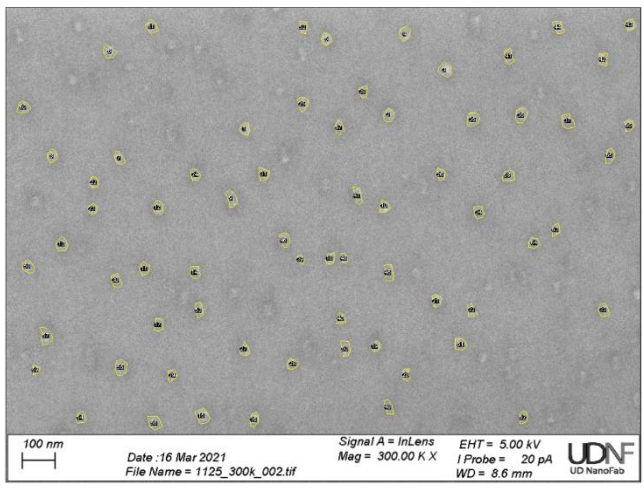
Sample #: 1124 | t_{Bi} = 60 s, T_{sub} = 275 °C | Date: 03/10/2021 | Sample plate: Q3 AFM Segmentation Mask parameters (Gaussian smoothing: 2.61 px, Add gradient: 5.10%, Add curvature: 39.84%, Barrier level: 76.47%, Prefill level: 60.94%, Prefill from minima: 39.16%





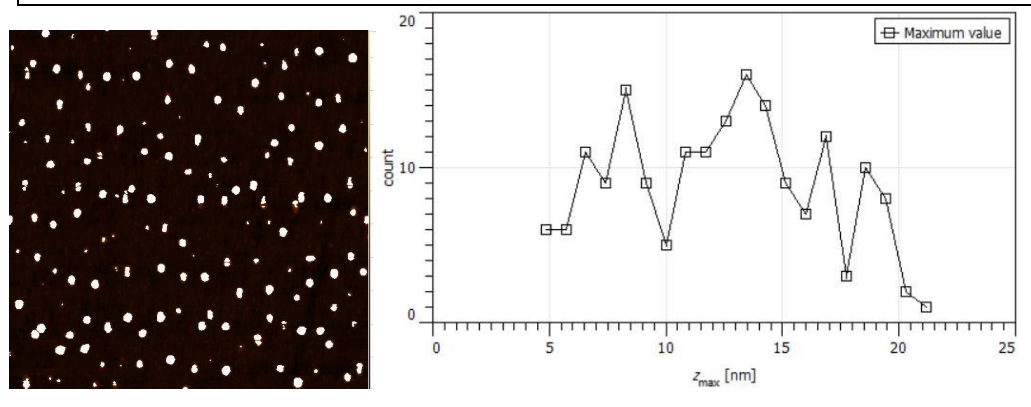
Sample #: 1125 | t_{Bi} = 60 s, T_{sub} = 275 °C | Date: 03/11/2021 | Sample plate: Q2 AFM Segmentation Mask parameters (Gaussian smoothing: 5.46 px, Add gradient: 8.81%, Add curvature: 62.38%, Barrier level: 57.86%, Prefill level: 27.31%, Prefill from minima: 16.52%

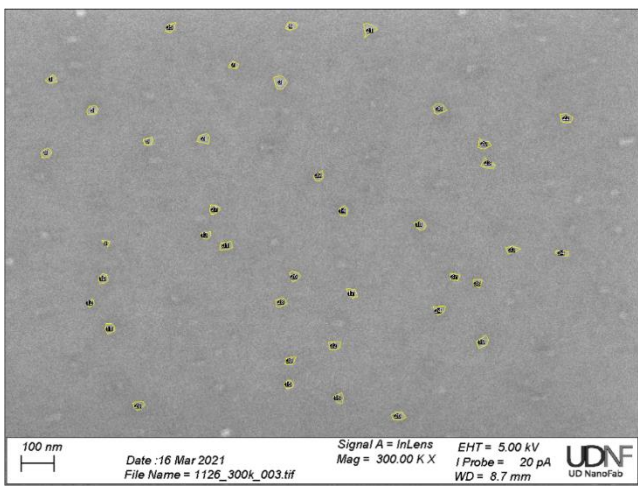




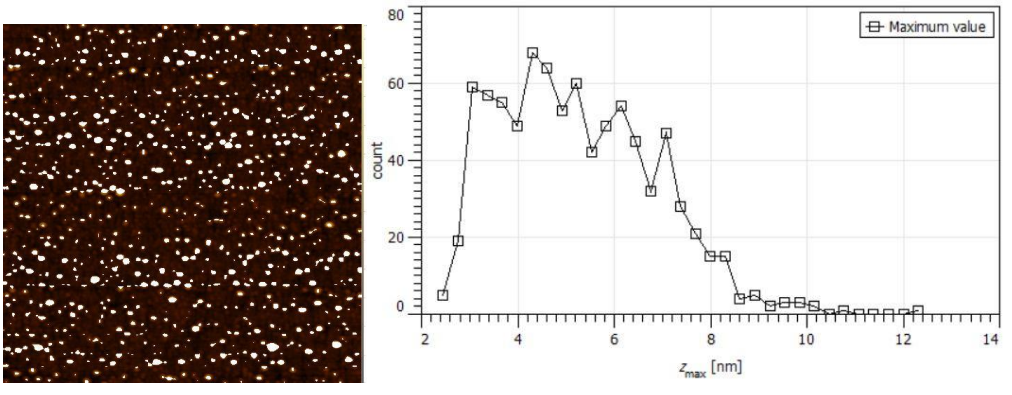
Sample #: 1126 | $t_{Bi} = 60 \text{ s}$, $T_{sub} = 285 \text{ °C}$ | Date: 03/11/2021 | Sample plate: Q3 AFM Segmentation Mask parameters (Gaussian smoothing: 2.00 px, Add gradient: 5.10%, Add curvature: 31.50%, Barrier level: 58.94%, Prefill level: 27.31%, Prefill from minima:

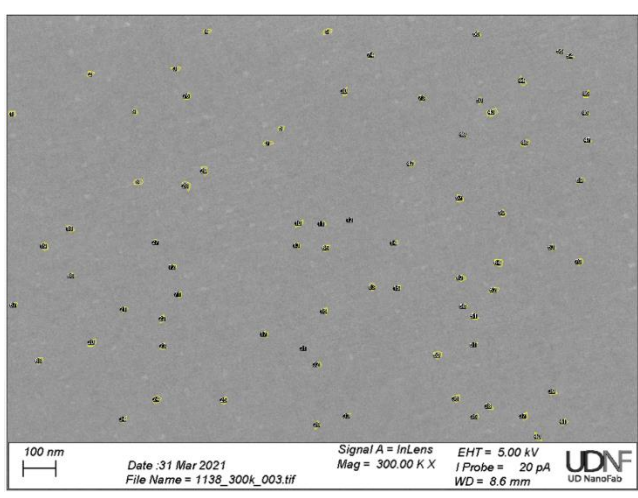
16.52%





Sample #: 1138 | t_{Bi} = 100 s, T_{sub} = 250 °C | Date: 03/23/2021 | Sample plate: Q3 AFM Segmentation Mask parameters (Gaussian smoothing: 5.06 px, Add gradient: 6.33%, Add curvature: 48.55%, Barrier level: 51.28%, Prefill level: 21.58%, Prefill from minima: 3.26%





<u>Section 3 – Discussing variables not directly controlled during growths</u>

While reflecting on the growth results, it was observed that some variables in the growth recipe were not strictly controlled for. Three such variables of potential interest were: A) duration substrate spent above 759 °C (presumed approximate deoxidation temperature of the GaAs wafers), B) duration substrate spent between 300 °C (closing of selenium shutter following deoxidation) and start of the growth, and C) duration substrate spent from the end of the growth until it was removed from the chamber. By using the digitized records of past growths, we were able to retrieve approximate values for these variables. Figure S8 is a graph showing the general variation in variables A) and C) for the growths presented in the main text. We note that variable B) will vary based on the substrate temperature desired for each respective growth but ranged anywhere from 11 to 27 minutes. The author recognizes the variance but does not attribute any of the main trends discussed in the main text to variations in these variables. However, controlling these variables may be of interest for future researchers who wish to work in this growth space.

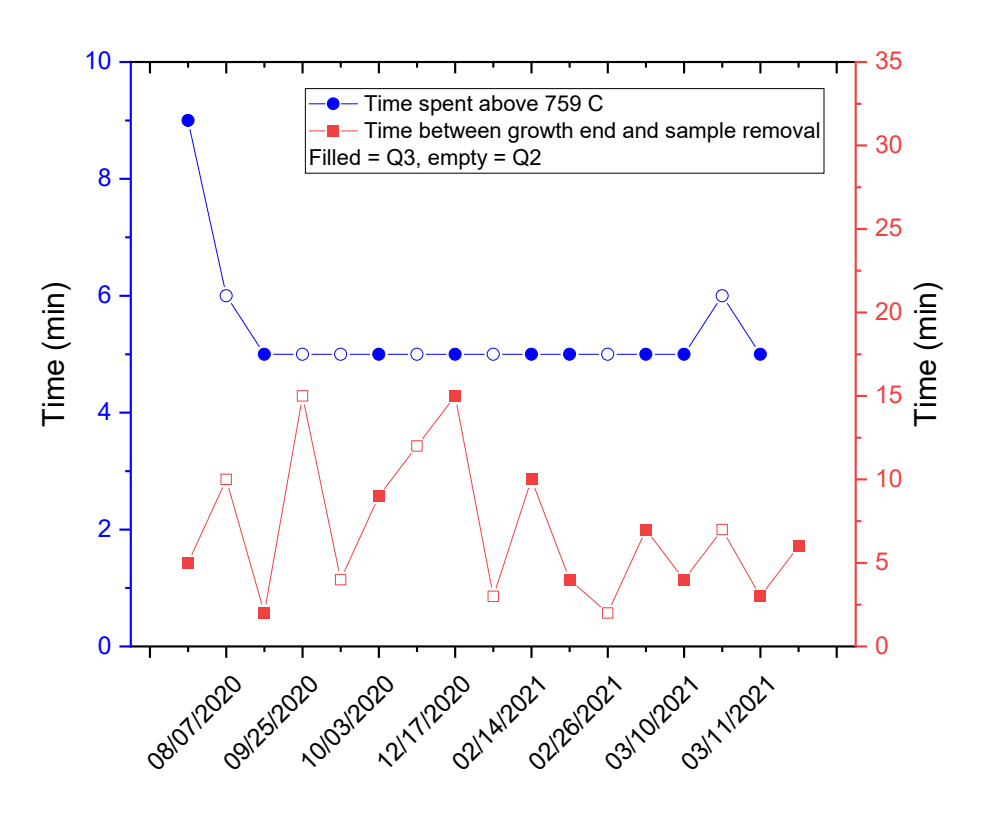


Figure S8: Variance in other variables not deliberately controlled during growth recipe.

Section 4 – Other features seen in AFM and SEM measurements

In addition to the nanoparticles of interest, there were other features present on our samples that would appear in the AFM and SEM images.

First are these streak-like features. Figure S9 is a $2x2 \mu m$ AFM scan of sample #898. We theorize that these are caused by mobile bismuth droplets travelling and leaving behind material. We note that in this and other instances, the streaks are perpendicular to the major flat of the wafer, and parallel to the direction of roughness in the underlying substrate.

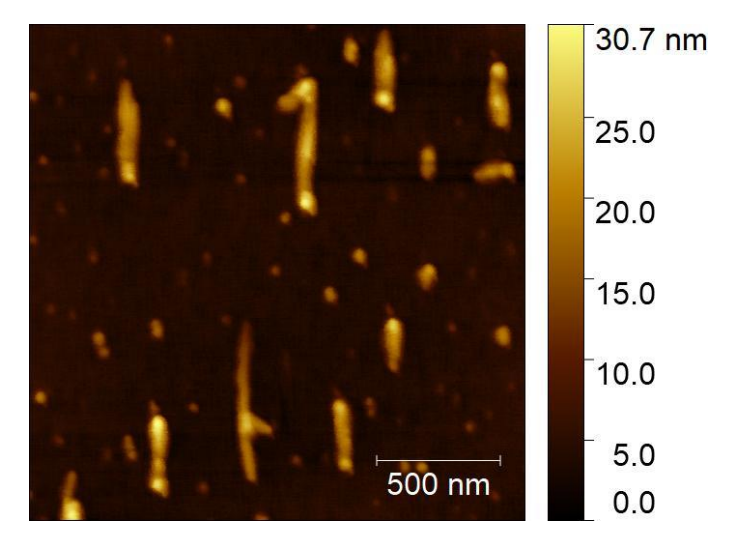


Figure S9: 2x2 µm image for sample #898. Streak-like features assumed to be mobile bismuth droplets.

Another feature which was seen consistently in SEMs were these clusters of material. Figure S10 is an SEM image of sample #920. They are seen at lower magnification and are both larger and provide more contrast than the nanoparticles studied. While they were seen consistently, we were unable to identify the origin or nature of these clusters.

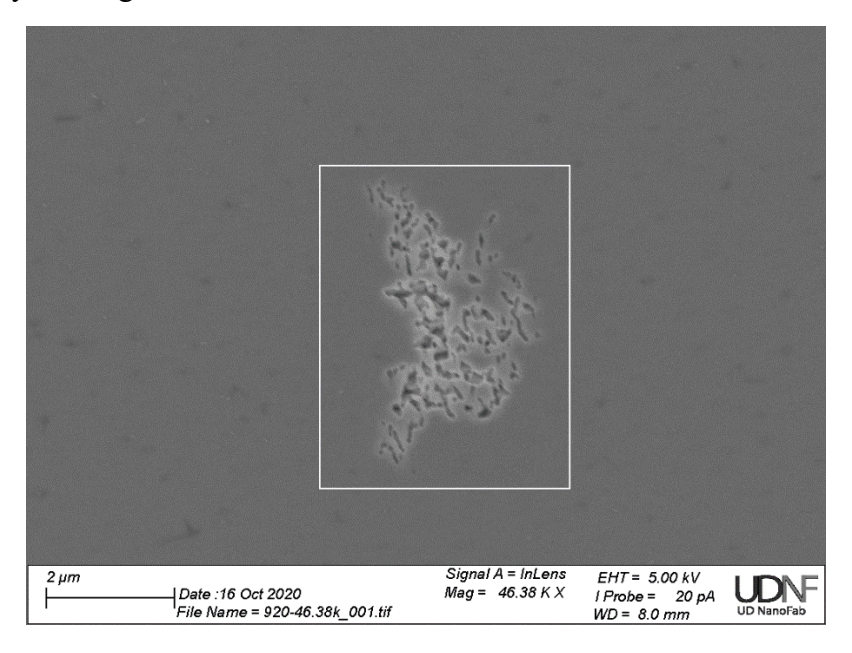


Figure S10: SEM image of sample #920. White box around cluster of material separate from the nanoparticles of interest.

We also observe on occasion long needle-like features. Again, they are seen at lower magnification due to their relative size, and their frequency and number are not consistent over a

single sample or between multiple samples. They are also not necessarily always aligned to the major flat of the underlying GaAs. It is possible that they are a specific growth mode of the bismuth or Bi_2Se_3 that occurs at specific temperatures, leading to their non-uniform appearance on the wafers. Needle-like morphologies have been observed in other Bi_2Se_3 growths and were attributed to the growth of the Bi_2Se_3 ($10\overline{1}5$) orientation¹.

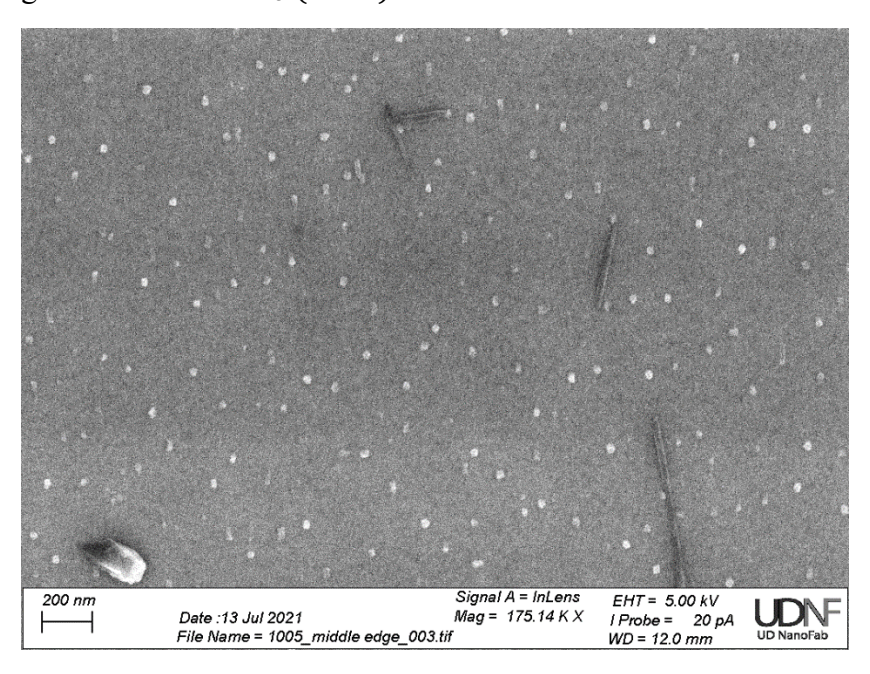


Figure S11: SEM image of sample #1005, showing the appearance of needle-like features.

Lastly, we occasionally observe highly circular features like those shown in Figure S12 which is an SEM image of sample #1050. These may be gallium droplets forming due to insufficient selenium overpressure. This interpretation is supported by the fact that these are commonly seen near or at the tab marks of our samples, though these features do sometimes appear closer to the center of the sample. This may be caused by the inability of the selenium overpressure to prevent all arsenic desorption, and subsequent gallium concentration and droplet formation.

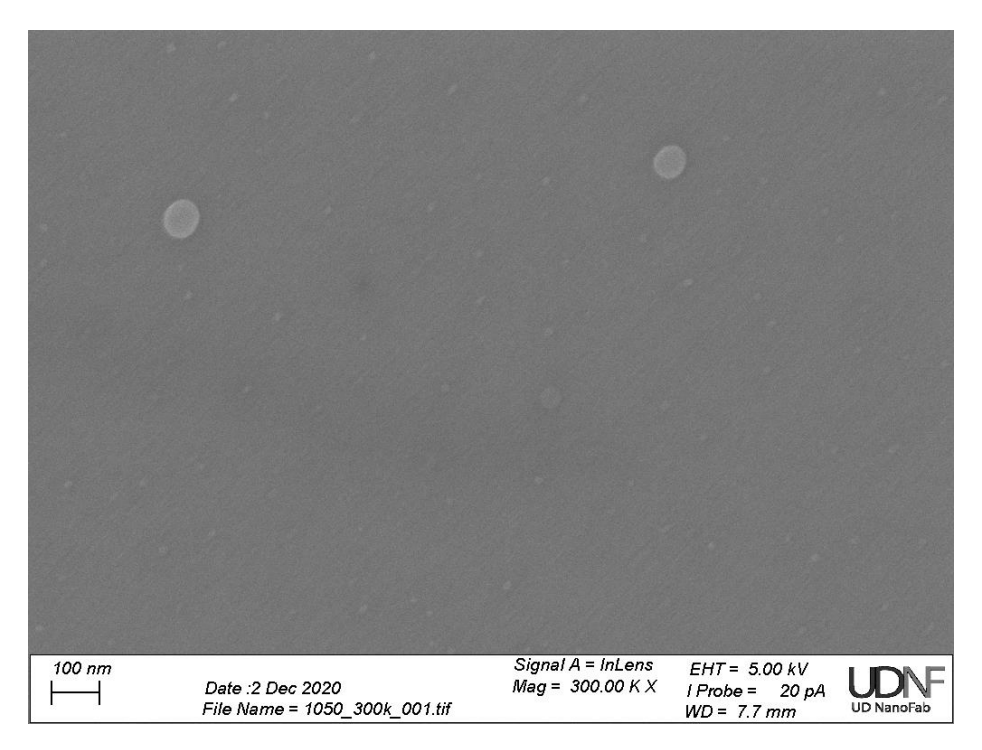


Figure S12: SEM image of sample #1050. Extremely circular particles assumed to be gallium droplets forming due to insufficient selenium overpressure, or inability to prevent all arsenic desorption.

References

¹ T.P. Ginley, Y. Zhang, C. Ni, and S. Law, J. Vac. Sci. Technol. A **38**, 023404 (2020).